Journal of the Korean Statistical Society
https://doi.org/10.1007/s42952-026-00374-2

Online ISSN 2005-2863
Print ISSN 1226-3192

RESEARCH ARTICLE

A bayesian non-parametric approach to dynamic conditional angular correlation model with application to portfolio optimization

Zhangshuang Sun[1] · Qian Li[1] · Haixiang Lin[2] · Guoqiang Wang[1]

Received: 18 August 2025 / Accepted: 5 April 2026

Abstract

In financial time series analysis, the dynamic conditional correlation model is the most popular method for estimating the conditional covariance matrix, which represents financial risk and is critical for risk management, portfolio optimization, and asset pricing. Traditional covariance matrix estimation is often constrained by the rigid parameter settings and the assumption of the normal distribution, leading to the estimation biases when the markets are not normally distributed. To address these limitations, this paper proposes a Bayesian Non-parametric Dynamic Conditional Angular Correlation model based on the Fractionally Integrated GARCH model (BNDCAC-FIGARCH) that incorporates the asymmetric parameter and the student's *t*-distribution to increase the adaptability and flexibility. Simulation experiments demonstrate that under overall correlation paths shaped as the sine or ramp functions, our model provides more accurate estimates, showcasing its effectiveness and stability. Empirical studies apply real stock market data, which includes DAX 40, FTSE 100, SSE 50, and CSI 100, to construct the portfolio optimization. The results demonstrate the superiority of the proposed model in terms of both portfolio returns and the reduction of parameter uncertainty. Furthermore, the results indicate that CSI 100 exhibits the weaker asymmetry compared to the other indices, likely due to its higher liquidity and a more accurate reflection of improved economic conditions resulting from national policies.

Keywords Covariance matrix estimation · Dynamic conditional angular correlation · Bayesian inference · GARCH · Portfolio optimization

Extended author information available on the last page of the article

Published online: 17 April 2026

1 Introduction

The estimation of the covariance matrix is one of the most crucial issues in modern statistics and econometrics, with applications in various fields such as economics, finance, and social sciences (see Engel et al. (2017); Li (2024)). Existing efforts of the traditional unconditional covariance matrix estimation and the related algorithms can be referenced to Zhou et al. (2015); Cai et al. (2016); Li and Xiao (2018) and Xiao et al. (2021). In the realm of finance, the construction of the covariance matrix for financial returns presents a more formidable challenge, as the covariance matrix not only exhibits time-varying characteristics but may also possess a considerably high dimensionality (So et al., 2018). These complexities require the use of more sophisticated statistical models to accurately capture the dynamic risks among assets. For instance, the multivariate generalized autoregressive conditional heteroskedasticity (GARCH) models provide a powerful tool for the risk management and the portfolio optimization by incorporating conditional heteroskedasticity. As an important branch of the multivariate GARCH models, Engle (2002) developed the dynamic conditional correlation (DCC) model to capture the conditional covariance matrix. However, when the size of the covariance matrix is excessively large, the DCC model shows unsatisfactory performance and even cannot be estimated due to computational problems, that is, it suffers from the curse of dimensionality (Engle et al., 2019). To alleviate the curse of dimensionality and accommodate richer correlation information, more extended models based on the DCC model have been developed, sucn as the dynamic conditional angular correlation (DCAC) model (Jarjour & Chan, 2020), the DCC model based on factor model (De Nard et al., 2021) and among others.

Furthermore, since real financial data often exhibit the asymmetry and fat-tailed characteristics, adopting a Bayesian approach can better align the model with the data, incorporating prior information into the parameters, and providing interpretations for those parameters (Nascimento et al., 2019). By leveraging prior knowledge and allowing for uncertainty in the estimates, the Bayesian approach can offer a more robust and informative framework for modeling financial time series. For the univariate GARCH model, Prass et al. (2016) explored the Bayesian inference of the fractionally integrated exponential GARCH model under the generalized error distribution, and elaborated on the interaction of the parameter prior settings by conducting simulation experiments on different parameter prior combinations. Sáfadi and Pereira (2010) constructed the Bayesian inference of the fractionally integrated asymmetric power GARCH model under the normal case, proved the adaptability of the model to the Bayesian approach through simulation experiments and empirical analysis, and proposed the future expectation of using heavy-tailed distribution. Furthermore, the Bayesian approaches for multivariate GARCH models (e.g. the DCC model) have been applied to multiple error distributions. For example, Fioruci et al. (2014) proposed a general process of Bayesian inference for multivariate GARCH models using skewed distribution, which enables the model to accommodate asymmetric heavy-tailed data and is closer to real financial data. Virbickaitė et al. (2016) presented a Bayesian non-parametric asymmetric DCC model utilizing errors modeled by an infinite Gaussian distribution with a positional scale mixture, which has been shown to have great flexibility in skewness and kurtosis. In addition, Virbickaitė

et al. (2015) reviewed the existing Bayesian inference of the univariate or the multivariable GARCH, and summarized the corresponding advantages and disadvantages, showing the effectiveness and flexibility of the Bayesian approaches compared with traditional parameter estimation. Recently, the above methods are applied in the intermarket systemic risk measures via the DCC model (see Shiferaw (2019); Tang and Aruga (2021); Goldman (2023) and Tukur (2024)), as well as more Bayesian approaches are extended and applied (i.e., Bauwens et al. (2014) and Meng et al. (2023)). In conclusion, the DCC model has been able to effectively measure the characteristics of non-normal distribution through the Bayesian method, but this method has not been fully explored in the DCAC framework. Even though the DCAC framework performs well in high kurtosis scenarios, it still fails to adequately quantify the non-normal distribution characteristics of the market.

Therefore, motivated by this underexplored potential in the DCAC framework, this study aims to address the deficiencies in modeling the non-normal distribution characteristics of the enhanced DCAC model (Sun et al., 2025), and makes the main contributions as follows: First, we propose the Bayesian non-parametric DCAC model based on the fractionally integrated GARCH model (BNDCAC-FIGARCH) to better account for the real financial data with non-normal distribution characteristics. The BNDCAC-FIGARCH model employs a Bayesian approach to estimate all unknown parameters and accommodates asymmetry in the distribution of error terms, thus providing a non-parametric extension to the DCAC-FIGARCH model. Secondly, we conduct simulation experiments to verify that Bayesian non-parametric methods can improve the accuracy of the correlation matrix estimation. Finally, we apply the BNDCAC-FIGARCH model to portfolio optimization, and a comparative analysis demonstrates that the model effectively captures non-normal distribution characteristics in real-world data, thereby enhancing the accuracy of financial risk measurement.

This paper is structured as follows: The BNDCAC-FIGARCH model and the detailed algorithm steps are constructed in Section 2. Some simulation studies are addressed to verify the accuracy of the proposed model in Section 3. The BNDCAC-FIGARCH model is employed in portfolio optimization to highlight the validity in practical applications in Section 4. Some conclusions and remarks are made in Section 5.

2 Methodology

In this section, we first review the structure of the DCAC-FIGARCH model and construct the corresponding Bayesian inference, resulting the BNDCAC-FIGARCH model. Then we provide the Markov Chain Monte Carlo (MCMC) algorithm steps for the parameter sampling. Finally, the predictive density can be derived to measure the performance of parameters and the volatility forecast.

2.1 The BNDCAC-FIGARCH model

To forecast the volatility of time series, Bollerslev (1986) first introduced the GARCH model as follows:

$$\begin{cases} r_t = \mu + \varepsilon_t, \\ \varepsilon_t = \sigma_t z_t, \\ \sigma_t^2 = \omega_0 + \sum_{i=1}^{q} \alpha_i \varepsilon_{t-i}^2 + \sum_{j=1}^{p} \beta_j \sigma_{t-j}^2, \end{cases} \tag{1}$$

where $p \geq 0$, $q > 0$, $\omega_0 > 0$, $\alpha_i \geq 0$, $\beta_j \geq 0$, and z_t follows the standard normal distribution. Moreover, considering the measurement of the long-term memory effects, the FIGARCH (1, d, 1) process is given by

$$\sigma_t^2 = \omega_0 + \beta_1 \sigma_{t-1}^2 + [1 - \beta_1 L - \phi_1(L)(1-L)^d]\varepsilon_t^2, \tag{2}$$

where $\omega_0 > 0$, L is the lag operator, $\alpha_1 > 0$, $\beta_1 > 0$, $\phi_1(L) = (1 - \alpha_1 L - \beta_1 L)(1-L)^{-1}$ to capture the short-term dynamics of the volatility shocks after fractionally differencing, and d characterizes the long memory property in volatility by allowing autocorrelations to decay at a slow hyperbolic rate with $0 < d < 1$.

With the increase of the asset dimension, the multivariate GARCH model is naturally expanded. For a multivariate time series $r_t = (r_{1t}, \ldots, r_{nt})'$, let $r_t = E[r_t|\mathcal{F}_{t-1}] + \varepsilon_t$, where $r_t|\mathcal{F}_{t-1} \sim N(0, H_t)$, $\mathcal{F}_{t-1} = \sigma(r_{t-1}, r_{t-2}, \ldots)$ denotes the sigma field generated by the past r_t and conditional on $\mathcal{F}_{t-1}$, and ε_t is the residual of the mean equation. Assume that the univariate variance follows the above FIGARCH (1, d, 1) process, the DCC matrix and covariance matrix estimation among multiple variables can be expressed as:

$$\begin{cases} \zeta_t = D_t^{-1} \varepsilon_t, \\ R_t = (1 - \theta_1 - \theta_2) R + \theta_1 \Gamma_{t-1} + \theta_2 R_{t-1}, \\ H_t = D_t R_t D_t, \end{cases} \tag{3}$$

where $D_t = \mathrm{diag}\{\sigma_t\}$, θ_1 and θ_2 are the ARCH effect and the GARCH effect parameters respectively with the constraints $\theta_1 \geq 0$, $\theta_2 \geq 0$, and $\theta_1 + \theta_2 < 1$ to maintain the stationarity of the positive conditional variance process. Γ_t is the conditional angular correlation matrix, which is defined by:

$$\Gamma_t = (\eta_t^{ij})_{n \times n} = \left(\frac{2\zeta_t^i \cdot \zeta_t^j}{(\zeta_t^i)^2 + (\zeta_t^j)^2} \right)_{n \times n}. \tag{4}$$

Here η_t^{ij} is the (i, j)th element of Γ_t, and ζ_t^i is the ith element of the standardized residual ζ_t in Equation (3). Equations (2) and (3) comprise the DCAC-FIGARCH model (Sun et al., 2025).

In general, the parameters of the correlation part can be estimated by the maximum likelihood estimation under the normality assumption. The log-likelihood function $\ell(\boldsymbol{\theta}_v, \boldsymbol{\theta}_c)$ of the DCAC model can be decomposed into two terms, i.e.,

$$\ell(\boldsymbol{\theta}_v, \boldsymbol{\theta}_c) := \ell_v(\boldsymbol{\theta}_v) + \ell_c(\boldsymbol{\theta}_v, \boldsymbol{\theta}_c), \tag{5}$$

where the functions $\ell_v(\cdot)$ and $\ell_c(\cdot, \cdot)$ represent the volatility term and the correlation term of the likelihood function. $\boldsymbol{\theta}_v$ is the vector of parameters involved in the volatility term of the likelihood (namely, $\omega_1, \omega_2, \ldots, \omega_n, \alpha_1, \alpha_2, \ldots, \alpha_n, \beta_1, \beta_2, \ldots, \beta_n, d$ in Equation (2)), and $\boldsymbol{\theta}_c$ is the vector of parameters involved in the correlation term of the likelihood (namely, θ_1 and θ_2 in Equation (3)). The volatility term and the correlation term are respectively given by

$$\ell_v\left(\boldsymbol{\theta}_v\right) = -\frac{1}{2}\sum_{t=1}^{T}\left(n\log(2\pi) + \log\left|D_t\right|^2 + \boldsymbol{\varepsilon}_t^{\top} D_t^{-1} D_t^{-1}\boldsymbol{\varepsilon}_t\right), \tag{6}$$

and

$$\ell_c\left(\boldsymbol{\theta}_v, \boldsymbol{\theta}_c\right) = -\frac{1}{2}\sum_{t=1}^{T}\left(\log\left|R_t\right| + \zeta_t^{\top} R_t^{-1}\zeta_t - \zeta_t^{\top}\zeta_t\right). \tag{7}$$

However, in most stock markets, the normality assumption cannot be satisfied. Therefore, we adopt a fully Bayesian approach to estimate all unknown parameters and allow for asymmetric distribution of the error terms.

Firstly, we assume that $v > 2$ so that H_t can always be interpreted as a conditional covariance matrix (Fioruci et al., 2014). The density function for this multivariate student's *t*-distribution is given by

$$p\left(\boldsymbol{x}\right) = \frac{\Gamma\left(\frac{\nu+k}{2}\right)}{\Gamma\left(\frac{\nu}{2}\right)\left[\pi(\nu-2)\right]^{k/2}}\left(1 + \frac{\boldsymbol{x}'\boldsymbol{x}}{\nu-2}\right)^{-\frac{\nu+k}{2}}. \tag{8}$$

Note that it is the standardized version of the multivariate student's *t*-distribution.

Secondly, to transform this continuous unimodal and symmetric distribution into a skewed one, we adopt the following class of skewed distributions (Fernández & Steel, 1998) indexed by a shape parameter $\gamma > 0$, which describes the degree of asymmetry, i.e.,

$$s(x \mid \gamma) = \frac{2}{\gamma + 1/\gamma}\left\{f\left(\frac{x}{\gamma}\right) I_{[0,\infty)}(x) + f(x\gamma) I_{(-\infty,0)}(x)\right\}, \tag{9}$$

where $f(\cdot)$ is a univariate density symmetric around zero and $I_C(\cdot)$ is an indicator function on C. Notably, $\gamma > 1$ means the right skewness while $\gamma < 1$ means the left skewness.

Finally, we can get the new standardized multivariate skew student's t-distribution, i.e.,

$$s(\boldsymbol{x} \mid \boldsymbol{\gamma}) = 2^k \left(\prod_{i=1}^{k} \frac{\gamma_i \sigma_{\gamma_i}}{1+\gamma_i^2} \right) \frac{\Gamma\left(\frac{\nu+k}{2}\right)}{\Gamma\left(\frac{\nu}{2}\right)[\pi(\nu-2)]^{k/2}} \left(1 + \frac{\boldsymbol{x}^* \boldsymbol{x}^*}{\nu-2}\right)^{-\frac{\nu+k}{2}}, \quad (10)$$

where

$$x_i^* = \begin{cases} (x_i \sigma_{\gamma_i} + \mu_{\gamma_i})/\gamma_i, & x_i \geq -\mu_{\gamma_i}/\sigma_{\gamma_i}, \\ (x_i \sigma_{\gamma_i} + \mu_{\gamma_i})\gamma_i, & x_i < -\mu_{\gamma_i}/\sigma_{\gamma_i}. \end{cases} \quad (11)$$

So, after the above procedures, we can describe the mean and the variance of the distribution as

$$\mu_\gamma = \frac{\Gamma((\nu-1)/2)\sqrt{\nu-2}(\gamma - 1/\gamma)}{\sqrt{\pi}\Gamma(\nu/2)}, \quad (12)$$

and

$$\sigma_\gamma^2 = \left(\gamma^2 + 1/\gamma^2\right) - \mu_\gamma^2 - 1, \quad (13)$$

respectively.

The corresponding likelihood function $\ell(\boldsymbol{\theta}_v, \boldsymbol{\theta}_c)$ under this distribution can be calculated through (denoted by $\ell(\theta)$):

$$\ell(\theta) = \prod_{t=1}^{n} |H_t|^{-1/2} p_\epsilon \left(H_t^{-1/2} \varepsilon_t\right) = \prod_{t=1}^{n} \left(\prod_{i=1}^{k} h_{ii,t}^{-1/2} \right) |R_t|^{-1/2} s(\varepsilon_t \mid \boldsymbol{\gamma}) \left((D_t R_t D_t)^{-1/2} \varepsilon_t\right). \quad (14)$$

Here Equation (14) establishes an essentially semi-parametric likelihood framework in which $s(\boldsymbol{x} \mid \boldsymbol{\gamma})$ dynamically governs the structure (see Long et al. (2011)). Although the formulation in Equation (14) assumes a parametric form of $s(\boldsymbol{x} \mid \boldsymbol{\gamma})$ for tractability, this component is inherently extensible. The structure allows $s(\boldsymbol{x} \mid \boldsymbol{\gamma})$ to be replaced by a non-parametric density estimator, such as a Dirichlet location–scale mixture of multivariate normals (Virbickaitė et al., 2016), thus providing a natural pathway from parametric to non-parametric modeling.

For the prior distributions of parameters, assuming that the univariate variance procedure is obtained by the FIGARCH model, the prior distributions of this part can be expressed as:

$$\begin{cases} \omega_i \sim N\left(\mu_{\omega_i}, \sigma^2_{\omega_i}\right) I_{(\omega_i>0)}, \\ \alpha_i \sim N\left(\mu_{\alpha_i}, \sigma^2_{\alpha_i}\right) I_{(0<\alpha_i<1)}, \\ \beta_i \sim N\left(\mu_{\beta_i}, \sigma^2_{\beta_i}\right) I_{(0<\beta_i<1)}, \ i = 1, \ldots, k. \\ d \sim N\left(\mu_d, \sigma^2_d\right) I_{(0<d<1)}, \\ \nu \sim N\left(\mu_\nu, \sigma^2_\nu\right) I_{(\nu>2)}, \end{cases} \tag{15}$$

Subsequently, a similar approach is adopted for the parameters θ_1 and θ_2 in (3), i.e., $\theta_1 \sim N\left(\mu_{\theta_1}, \sigma^2_{\theta_1}\right) I_{(0<\theta_1<1)}$ and $\theta_2 \sim N\left(\mu_{\theta_2}, \sigma^2_{\theta_2}\right) I_{(0<\theta_2<1)}$. As for the skewness parameters, we shall assume that the parameter vector γ is independent and use a *Gamma*(a, b) prior on each γ_i^2.

Since the posterior distribution is analytically intractable under a *t*-distributed error assumption (see Fioruci et al. (2014)), we directly adopt MCMC sampling strategies for obtaining samples. The following figure illustrates the hierarchical structure of the model parameters and the generative process of the joint distribution of the data and priors.

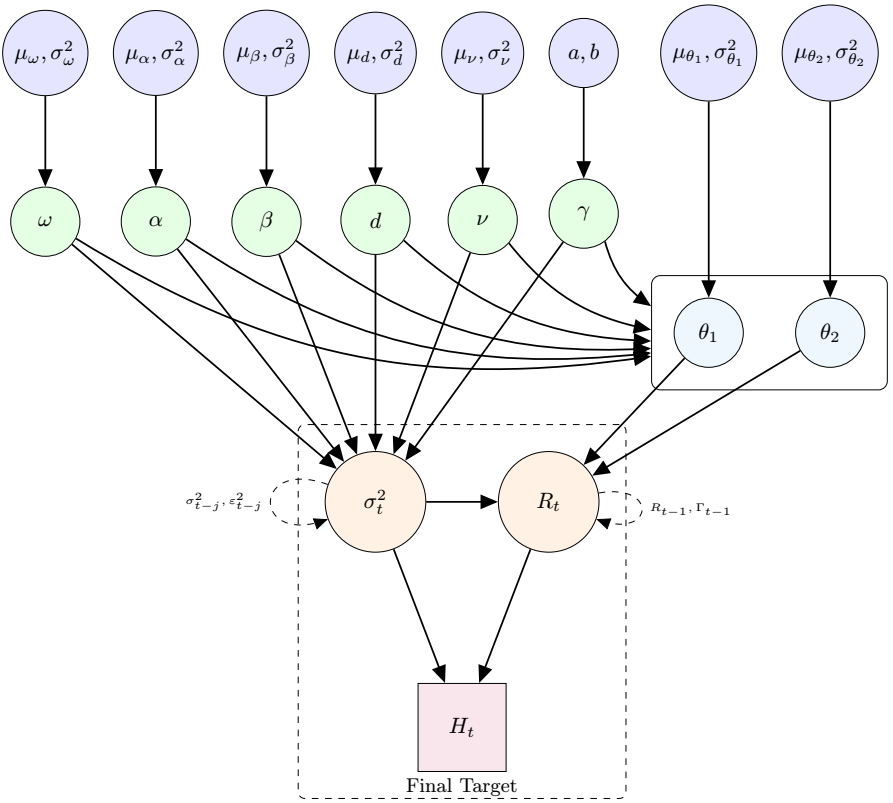

Fig. 1 Hierarchical structure of the Bayesian DCAC-FIGARCH model

2.2 MCMC algorithm

For the parameter estimation algorithm, this section adopts the ensemble sampler strategy based on the Metropolis-Hastings criterion. The following describes the process in detail:

- Step 1 Preparation: Apply the model proposed by (2) and (3), construct the likelihood function $\ell(\theta)$ as:

$$\ell(\theta) = \prod_{t=1}^{n} \left(\prod_{i=1}^{k} h_{ii,t}^{-1/2} \right) |R_t|^{-1/2} s(\varepsilon_t \mid \boldsymbol{\gamma}) \left((D_t R_t D_t)^{-1/2} \varepsilon_t \right), \tag{16}$$

and set the prior distributions as:

$$\begin{cases} \omega_i \sim N\left(\mu_{\omega_i}, \sigma_{\omega_i}^2\right) I_{(\omega_i>0)}, \\ \alpha_i \sim N\left(\mu_{\alpha_i}, \sigma_{\alpha_i}^2\right) I_{(0<\alpha_i<1)}, \\ \beta_i \sim N\left(\mu_{\beta_i}, \sigma_{\beta_i}^2\right) I_{(0<\beta_i<1)}, \\ d \sim N\left(\mu_d, \sigma_d^2\right) I_{(0<d<1)}, \\ \nu \sim N\left(\mu_\nu, \sigma_\nu^2\right) I_{(\nu>2)}, \\ \theta_1 \sim N\left(\mu_{\theta_1}, \sigma_{\theta_1}^2\right) I_{(0<\theta_1<1)}, \\ \theta_2 \sim N\left(\mu_{\theta_2}, \sigma_{\theta_2}^2\right) I_{(0<\theta_2<1)}, \\ \gamma_i^2 \sim Gamma(a, b), \end{cases} \quad i = 1, \ldots, k; \tag{17}$$

- Step 2 Initialization: Randomly generate multiple initial states; set sampler parameters including the number of walkers (walkers=20), movement strategy (chain_length=1250, record_interval=5) and burn-in amount (burn=chain _length×20%);
- Step 3 Parallel exploration: Starting from different initial positions, calculate the likelihood function, prior probability and posterior probability respectively as above;
- Step 4 Acceptance probability calculation: Calculate the acceptance probability based on the current state x_t and the candidate state x' as follows:

$$\alpha(x_t, x') = \min\left\{1, \frac{\pi(x')s(x_t|x')}{\pi(x_t)s(x'|x_t)}\right\}, \tag{18}$$

where $\pi(x)$ is the target distribution, $s(x)$ is the probability density function (10);

- Step 5 State update: Select a random number $u \sim U(0,1)$. If $\alpha(x_t, x') \geq u$, let $x_{t+1} = x'$, that is, accept the candidate state; if $\alpha(x_t, x') < u$, let $x_{t+1} = x_t$, that is, reject the candidate state and keep it unchanged;
- Step 6 Post-processing: Remove the burn-in period samples, merge the Markov chain, and obtain parameter samples.

After the above process, we obtain Markov chains with different parameters, and calculate their autocorrelation time to determine whether they have reached convergence. From this, we can estimate the posterior distribution of the parameters, including information such as the mean, variance, and confidence interval, and thus obtain the parameter estimates of the model.

To evaluate the model performance, we focus on the one-step-ahead predictive density of the returns, which is given by

$$f\left(r_{T+1} \mid r^{T}\right)=\int f\left(r_{T+1} \mid \Theta, r^{T}\right) f\left(\Theta \mid r^{T}\right) d\Theta, \tag{19}$$

where the integral can be approximated by the output of the MCMC algorithm, i.e.,

$$\frac{1}{M} \sum_{m=1}^{M} f\left(r_{T+1} \mid \Theta^{(m)}, r^{T}\right). \tag{20}$$

Here M is the length of the Markov chains.

3 Simulation study

In this section, we will construct a simulated data set to estimate the DCC matrix and begin to study the performance of the BNDCAC-FIGARCH model. In order to effectively solve the proposed problem, we generate a binary time series consisting of 1000 observations, with available volatility through the standard GARCH (1,1) model, and the parameters and model settings are as follows:

$$\begin{cases} \sigma_{1,t}^{2} & =0.01+0.05\varepsilon_{1,t-1}^{2}+0.94\sigma_{1,t-1}^{2}, \\ \sigma_{2,t}^{2} & =0.5+0.2\varepsilon_{2,t-1}^{2}+0.5\sigma_{2,t-1}^{2}. \end{cases} \tag{21}$$

It is worth noting that, we set ε_t to follow the student's t-distribution independently and identically distributed. That is, the innovation of the mean equation satisfies the student's t-distribution. The asymmetric parameter γ is set to be 1 to compare the effects of the distribution features. Furthermore, we set the overall correlation coefficient ρ_t to the following various procedures (Engle, 2002):

$$\begin{cases} \text{constant:} & \rho_{constant,t}=0.9, \\ \text{sine:} & \rho_{sine,t}=0.5+0.4\cos(2\pi t/200), \\ \text{fast sine:} & \rho_{fastsine,t}=0.5+0.4\cos(2\pi t/20), \\ \text{ramp:} & \rho_{ramp,t}=(t \bmod 200)/200, \\ \text{step:} & \rho_{step,t}=0.9-0.5I(t>500), \end{cases} \tag{22}$$

where $I(\cdot)$ is the indicative function.

Table 1 and Figs. 2, 3, 4, 5 and 6 present the parameter estimation results and evolution trace of different models during the aforementioned simulation process, respectively.

Specifically, Table 1 summarizes the correlation parameter estimation outcomes and precision evaluations of the models, including the mean squared error (MSE), the mean absolute error (MAE) and the root mean squared error (RMSE). Note that all metrics reported here evaluate the accuracy of the correlation estimates. Considering that the residuals are assumed to follow a student's *t*-distribution, we focus more on MAE which mitigates the impact of the individual outliers arising from the non-normal distribution characteristics. The findings demonstrate that under the assumption of non-normal distributed innovations, the BNDCAC-FIGARCH model exhibits superior forecasting performance compared to alternative parametric methods when correlation coefficient paths exhibit sine-type (ρ_{sine}) and ramp-type (ρ_{ramp}) characteristics. For instance, under ramp-type correlation coefficient ρ_{ramp} conditions, the BNDCAC-FIGARCH model reduces MAE of conditional correlation matrices by approximately 7.90% compared to conventional parametric models. On the other hand, for the constant-, fast sine-, and step-type correlation coefficient conditions, the BNDCAC-FIGARCH model fails to achieve notable improvements. This may be attributed to its increased model complexity, which introduces the unnecessary fac-

Table 1 Parameter estimation results and correlation matrix estimation evaluation

Model	θ_1	θ_2	MSE	MAE	RMSE
$\rho_{constant}$					
DCC	0.00000	0.97725	0.00000	0.00000	0.00000
DCAC-GARCH	0.01442	0.65767	0.00000	0.00266	0.00702
DCAC-FIGARCH	0.01339	0.64447	0.00004	0.00237	0.00633
BNDCAC-FIGARCH	0.45812	0.29910	0.02126	0.04438	0.14582
ρ_{sine}					
DCC	0.08194	0.89962	0.01732	0.05485	0.13161
DCAC-GARCH	0.09627	0.88761	0.01675	0.05272	0.12943
DCAC-FIGARCH	0.09674	0.88761	0.01684	0.05287	0.12977
BNDCAC-FIGARCH	0.03481	0.25957	0.00017	0.00538	0.01322
$\rho_{fastsine}$					
DCC	0.00244	0.98435	0.00003	0.00220	0.00570
DCAC-GARCH	0.08280	0.53710	0.00154	0.01548	0.03926
DCAC-FIGARCH	0.08085	0.53889	0.00147	0.01514	0.03840
BNDCAC-FIGARCH	0.16298	0.65465	0.00816	0.03569	0.09031
ρ_{ramp}					
DCC	0.07553	0.90406	0.01307	0.04897	0.11432
DCAC-GARCH	0.10000	0.77276	0.00675	0.03245	0.08216
DCAC-FIGARCH	0.10000	0.77140	0.00668	0.03227	0.08173
BNDCAC-FIGARCH	0.01819	0.88889	0.00588	0.02972	0.07669
ρ_{step}					
DCC	0.02030	0.97615	0.00907	0.04480	0.09524
DCAC-GARCH	0.04393	0.89832	0.00513	0.02798	0.07162
DCAC-FIGARCH	0.04297	0.89991	0.00507	0.02783	0.07123
BNDCAC-FIGARCH	0.26265	0.33949	0.01116	0.03882	0.10565

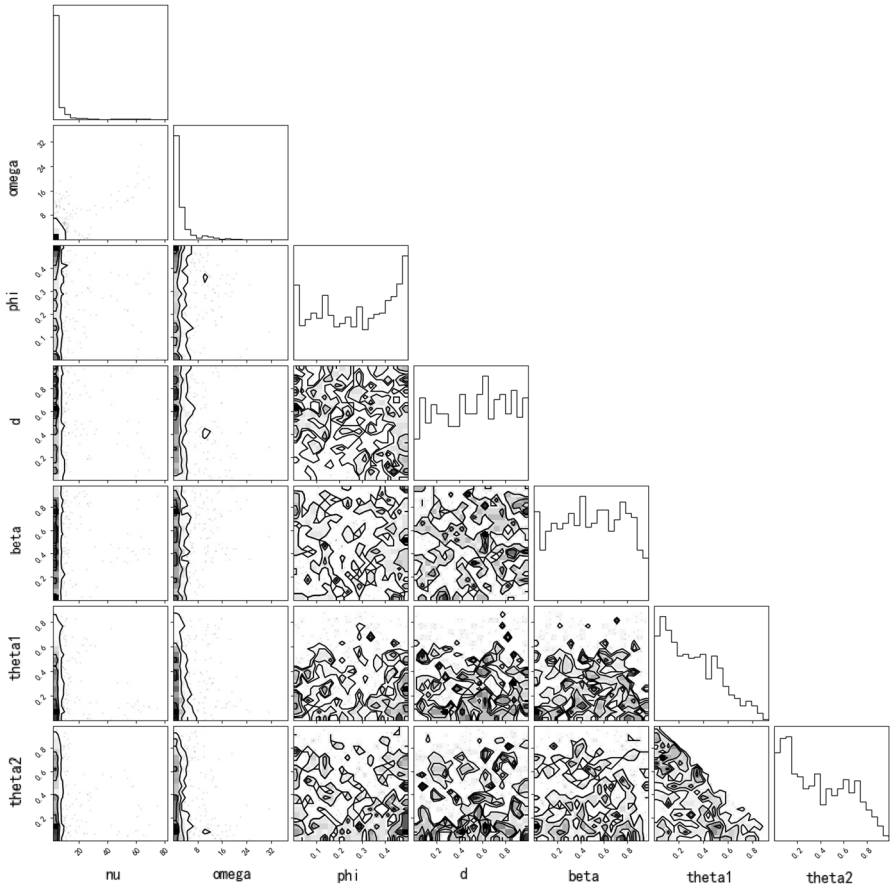

Fig. 2 The parameter marginal distribution and corner diagram under $\rho_{contant}$

tors in the aforementioned simple scenarios where classical models such as the DCC model already perform satisfactorily.

To further investigate this phenomenon, we conduct a more in-depth analysis. It is worth noting that the BNDCAC-FIGARCH model performs exceptionally well under the slowly varying ρ_{sine} process but poorly under the rapidly oscillating ρ_{fastsine} scenario. This contrast arises because the FIGARCH component is designed to capture long-memory dynamics characterized by a slow decay of autocorrelations, making it effective for modeling persistent, low-frequency fluctuations. In contrast, the fastsine process requires rapid adaptation to frequent changes, which conflicts with the inherent smoothing properties of both the FIGARCH filter and the Bayesian nonparametric clustering mechanism (see Belkhouja and Boutahary (2011) and Anyah et al. (2025)). As a result, the model exhibits delayed responses and larger prediction errors in rapid-change environments. This suggests that BNDCAC-FIGARCH is best applied in contexts where correlations evolve gradually over time without frequent abrupt shifts.

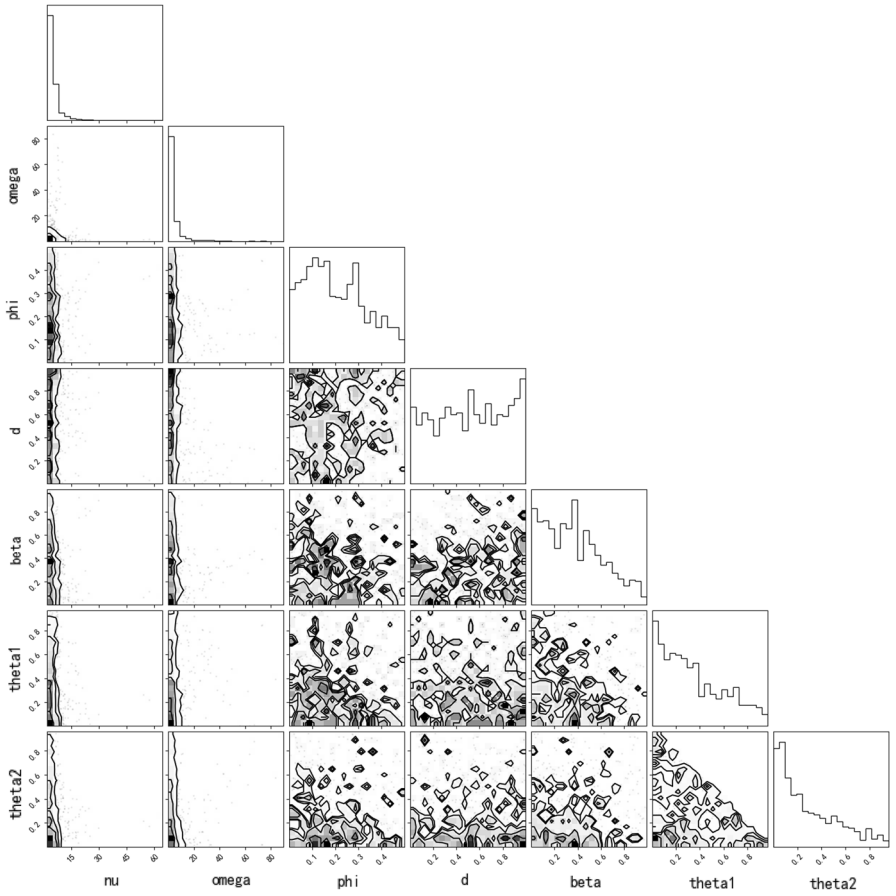

Fig. 3 The parameter marginal distribution and corner diagram ρ_{sine}

Furthermore, Figs. 2, 3, 4, 5 and 6 illustrate the posterior marginal distributions of parameters, parameter correlations, and Markov chain traces. The parameter correlation plots in Figs. 2, 3 and 4 reveal no statistically significant correlations among most parameters, indicating independence characteristics in the estimation outcomes. Notably, under the ρ_{sine} and ρ_{ramp} correlation coefficient paths where the BND-CAC-FIGARCH model demonstrates superior performance, a pronounced negative linear relationship emerges between parameters θ_1 and β: systematic decay of θ_1 accompanies increasing β.

Theoretically, θ_1 governs the short-term memory effects in cross-asset correlations, while β quantifies volatility persistence in short-term memory. Enhanced volatility persistence amplifies intrinsic volatility clustering, consequently elevating uncertainty in cross-asset correlation forecasting. The observed attenuation of θ_1 precisely reflects the weakening mechanism of correlation-related short-term memory effects. By simultaneously estimating parameter interdependencies and marginal distributions, this framework effectively quantifies uncertainties inherent to such

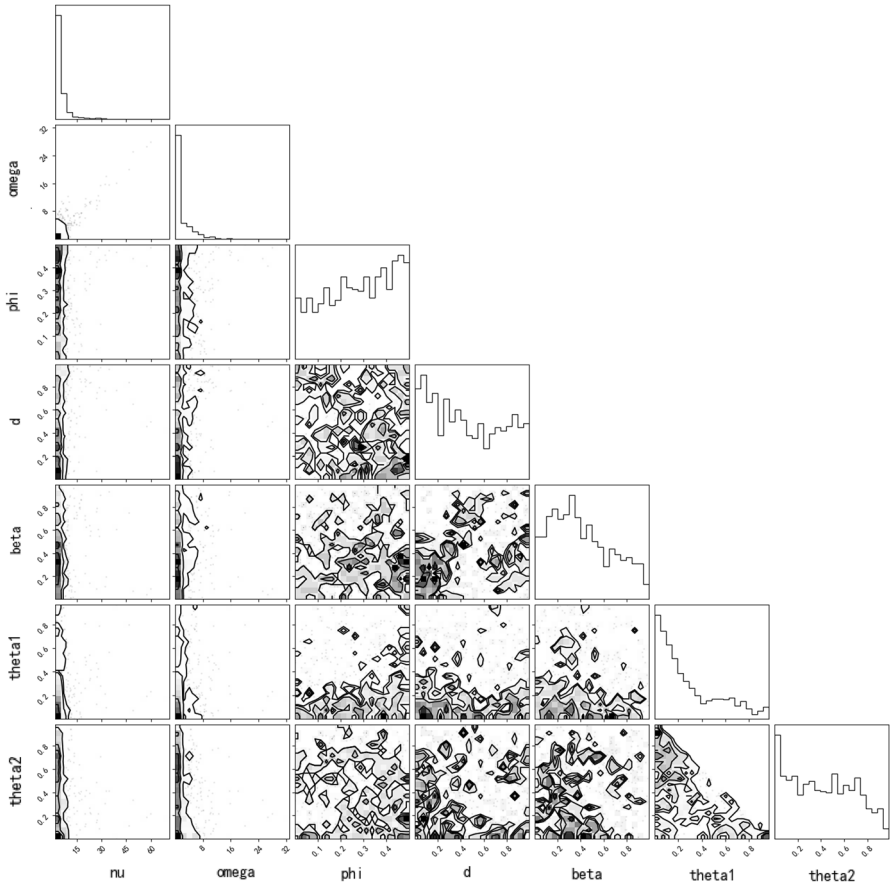

Fig. 4 The parameter marginal distribution and corner diagram under ρ_{ramp}

interactions, thereby demonstrating its modeling superiority in complex financial ecosystems characterized by intricate volatility-correlation dynamics.

From Fig. 5, the trace plots of the MCMC chains exhibit stable, nearly horizontal fluctuations after an initial period, indicating that the chains have converged to their stationary distributions (see Brooks et al. (2003) and Sinharay (2003)). During the evolution of ramp-type correlation coefficient (ρ_{ramp}), the volatility parameters ν, β, and d converge to stable values of 2.70, 0.18, and 0.99, respectively, with correlation parameters θ_1 and θ_2 asymptotically approaching 0.02 and 0.89. In this scenario, the model achieves the minimum MAE in correlation coefficient estimation among all comparative frameworks, indicating that the BNDCAC-FIGARCH model effectively mitigates parameter estimation uncertainty and enhances modeling accuracy for market volatility and risk quantification in environments characterized by non-normal distributions and rapid cyclical variations.

Finally, Bayesian inference results (see Fig. 6) reveal that the posterior distributions exhibit markedly leptokurtic features compared to the prior normal specifications, with parameters θ_1 and θ_2 demonstrating asymmetric heavy-tailed distributions.

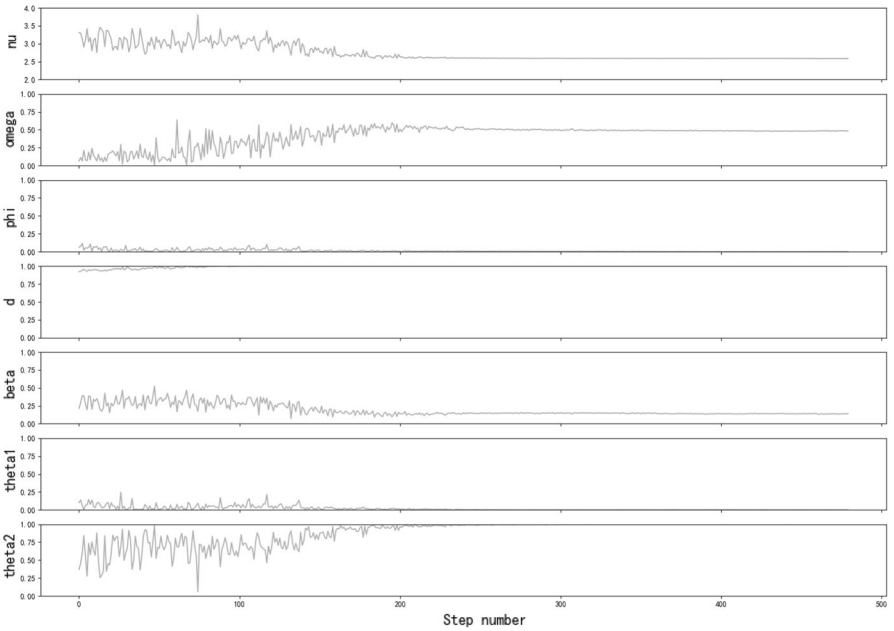

Fig. 5 The parameter trace under ρ_{ramp}

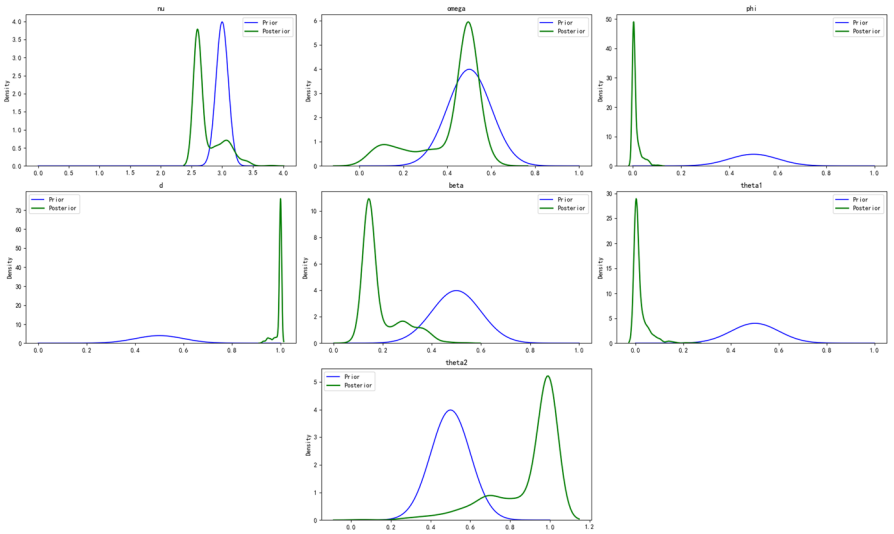

Fig. 6 The posterior distribution of parameters under ρ_{ramp}

These findings substantiate the enhanced parameter identification capability of the BNDCAC-FIGARCH model: its estimation outcomes not only achieve precise convergence to the true parameter space but also recover the parameters' intricate statistical signatures and distributional complexities.

4 Real data analysis

In this section, we utilize the global stocks indices as test cases for the empirical research on the portfolio optimization. The previous section constructed the BNDCAC-FIGARCH model and the simulation study to extend the applicability of the original model to non-normal financial data. Building on these theoretical and simulation-based results, we now evaluate the model's practical performance using real-world financial market data.

4.1 Datasets

To validate the effectiveness of the proposed model in portfolio optimization applications, this section employs the DAX 40, FTSE 100, SSE 50 and CSI 100 stock datasets for application analysis, sourced from Google Finance (https://www.google.com/finance) and the Tushare platform (https://www.tushare.pro). Additionally, the descriptive statistics and Jarque-Bera (*JB*) test results of the above stock index components are shown in Table 2.

4.2 Portfolio design

In portfolio optimization, many efforts have already been made to establish the strategy benchmarks (e.g., Cai et al. (2000); Li et al. (2021) and Li et al. (2022)). To evaluate the out-of-sample performance of the BNDCAC-FIGARCH model, we adopt the Global Minimum Variance (GMV) portfolio as a benchmark. When the covariance matrix possesses desirable properties, this portfolio strategy can achieve the minimal variance (Engle et al., 2006). The associated optimization model can be formulated as:

$$\begin{aligned} &\min \omega^{'} \Sigma \omega, \\ &\text{s.t.} \begin{cases} \omega^{'} r_t = r_{target}, \\ \omega^{'} I = 1, \end{cases} \end{aligned} \tag{23}$$

where ω represents the asset weight and r_{target} denotes the predefined return target. Notably, ω may take negative values due to the permission of shorting. For the return target, we select the higher of the historical average return and the weighted average return, where the latter is based on the weighting methodology of the stock index. Meanwhile, existing extended parametric models based on the DCC model are

Table 2 Statistical analysis for constituent stocks of stock index

Index	Mean × 10^{-2}	Min	Max	Std × 10^{-2}	Skewness	Excess kurtosis	*JB* value
DAX 40	0.0428	-0.3375	0.4000	2.1871	-0.0351	11.7043	3854.2544*
FTSE 100	0.0350	-0.5000	2.2847	2.2088	0.1318	18.6676	5611.5399*
SSE 50	0.0284	-0.6461	0.2012	1.7851	2.3436	9.6593	4181.4463*
CSI 100	0.0331	-0.5170	0.3035	1.8649	1.5853	3.6641	463.3307*

Note: '*' indicates the *JB* statistic value of the main component of the index

used for comparison, including the DCC model (Engle, 2002), the DCAC-GARCH model (Jarjour & Chan, 2020) and the DCAC-FIGARCH model (Sun et al., 2025).

4.3 Out-of-sample performance analysis

In order to compare the out-of-sample performance of different models, this section presents the results of the model parameter estimation and portfolio optimization for the aforementioned four datasets. Notably, we use annualized average return (AV), annualized standard deviation (SD), information ratio (IR) and Sharpe ratio (SR) as the evaluation criteria for the out-of-sample performance of the portfolio. AV reflects the profitability of the portfolio strategy, with a higher AV indicating that the model enables more profitable asset allocation by accurately capturing dynamic correlation changes. SD measures portfolio risk, and a lower SD indicates effective diversification. IR, defined as the ratio of AV to SD, assesses the magnitude of excess return per unit of risk: higher IR signifies greater practical advantage. SR further evaluates the excess return per unit of risk relative to the risk-free rate, providing a comprehensive measure of risk-adjusted performance: a higher SR implies superior economic value through enhanced returns and controlled risks. Under the GMV framework, these metrics directly reflect the quality of the estimated covariance matrix (De Nard et al., 2022). Furthermore, the most critical out-of-sample performance measures we focus on are SD and SR, whose relative importance depends on the investor type.

4.3.1 DAX 40

For DAX 40, Fig. 7 presents the posterior marginal distributions and parameter correlations estimated by the BNDCAC-FIGARCH model, with the corresponding sampling trace plots shown in Fig. 8.

From Fig. 7, the empirical results reveal that the joint distributions of volatility parameters (β, ϕ, d) and correlation parameters (θ_1, θ_2) exhibit no significant covariation characteristics, manifested through dispersed posterior density contours between parameters.

More importantly, the joint posterior distribution of θ_1 and θ_2 demonstrates marked clustering in the lower-left region of parameter space, forming triangular contour patterns that suggest potential nonlinear coupling mechanisms between them. This nonlinear relationship may originate from time-varying characteristics in cross-asset volatility transmission. In addition, Fig. 8 displays the trace plots of posterior parameter sampling, indicating statistically significant convergence properties. As shown in Fig. 8, all parameters exhibit stationary and ergodic fluctuations with diminishing amplitudes after removing burn-in periods, with particularly pronounced convergence in the θ_2 trace. These patterns confirm that the BNDCAC-FIGARCH model satisfies asymptotic stability requirements, ensuring estimation reliability. The periodic fluctuations of parameters likely stem from dual constraints: the inherent needs of the model's dynamic time-varying attributes and the finite sampling frequency. The trace plot exhibits seemingly periodic fluctuations, but in fact shows oscillations around a stable mean, indicating the good mixing and reliable estimation. This pattern may arise from random-walk behavior near parameter boundary constraints, leading to

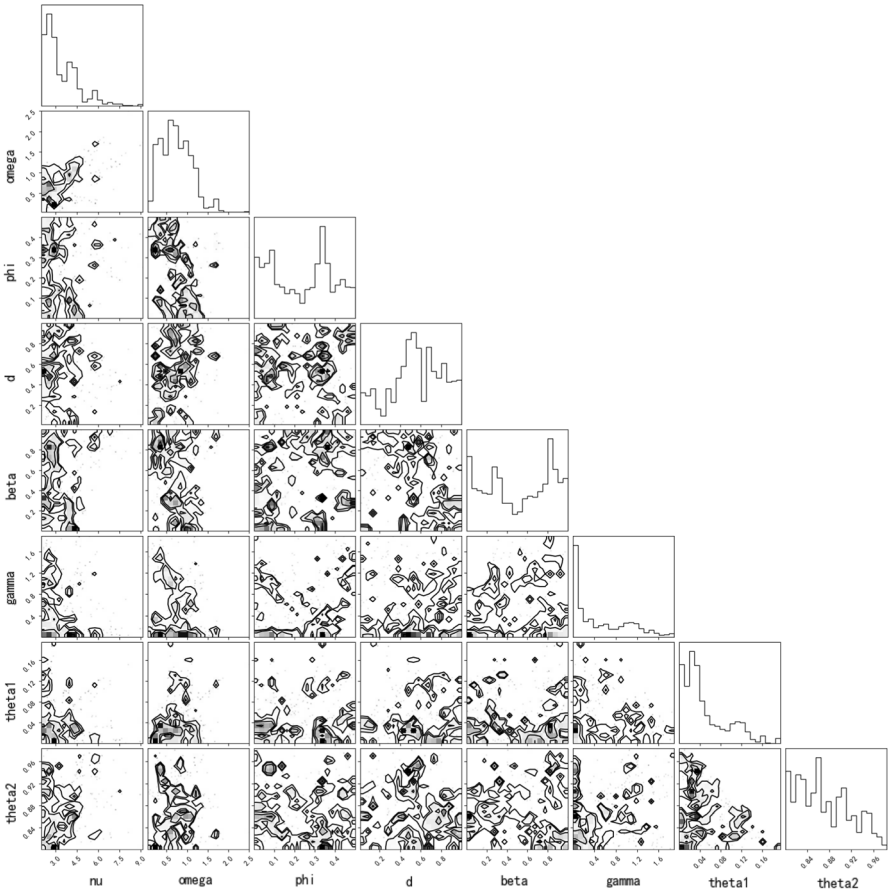

Fig. 7 The parameter marginal distribution and corner diagram in DAX 40

"pseudo-periodicity" and suggesting that the constrained parameter space could be further tightened to improve estimation efficiency (Nakajima & Omori, 2012). These findings not only validate the model's parameter identification mechanism but also underscore the necessity of rigorous convergence diagnostic procedures in complex financial econometric models.

A comparison of the posterior and prior distributions of the model parameters is shown in Fig. 9. The posterior distributions of parameters (β, ϕ and d) exhibit lower peaks and broader spreads compared to their prior distributions, while the posterior distributions of θ_1 and θ_2 demonstrate more pronounced sharp peaks and heavier tails. This corroborates the parameter discrepancies observed in the corner plot, indicating that correlation parameters in financial markets are more susceptible to the influence of return characteristics.

Table 3 summarizes the parameter estimation results of the BNDCAC-FIGARCH model for DAX 40. The long-memory response parameters ϕ and d both exceed theoretical thresholds for long-memory features, confirming the significant long-memory effects in DAX 40. For the distribution shape parameter ν, all values are strictly

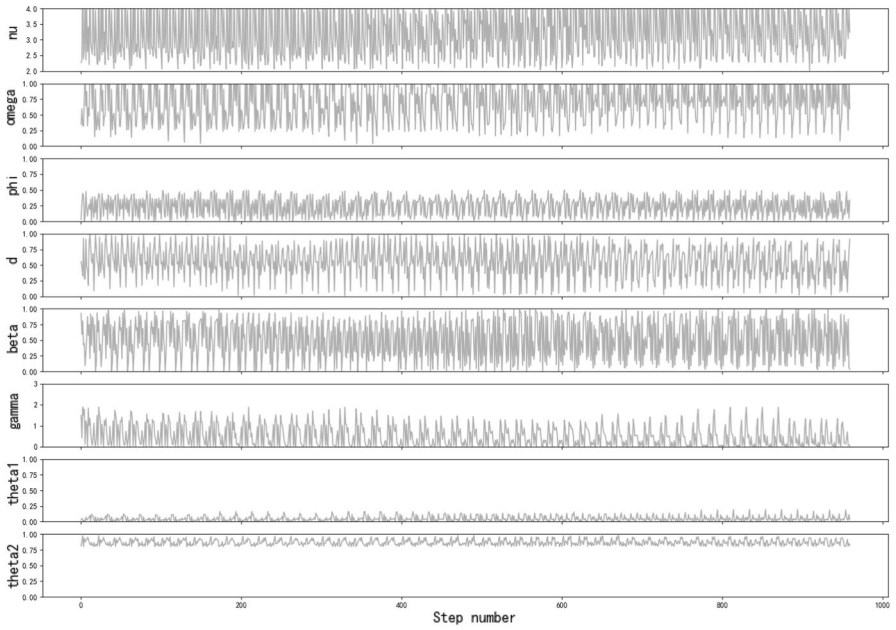

Fig. 8 The parameter trace in DAX 40

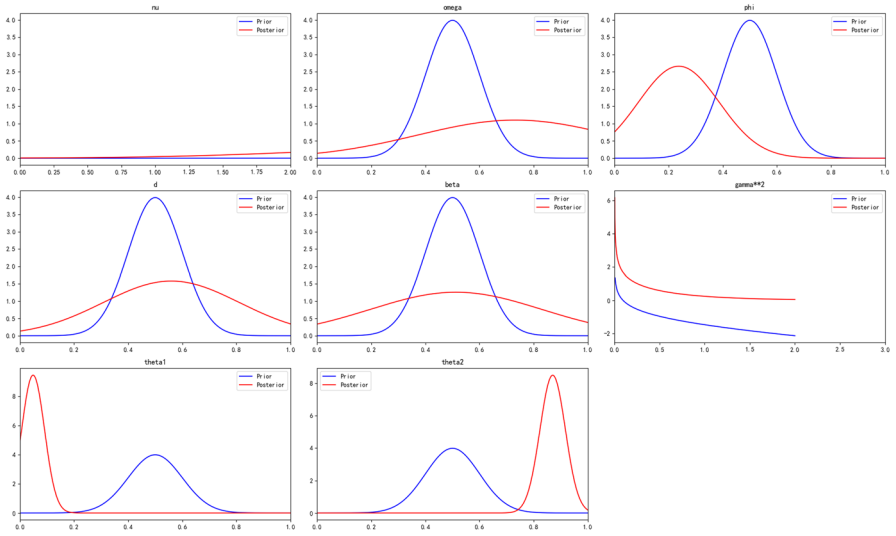

Fig. 9 The posterior distribution compared with the prior distribution in DAX 40

greater than 2, reflecting the heavy-tailed characteristics and ensuring the validity of the high-dimensional covariance matrix estimated by the model. The combined mean of correlation parameters $\theta_1 + \theta_2$ reaches 0.91, suggesting substantial persistent influence of historical data on volatility and covariance matrix predictions. Addi-

Table 3 Parameter estimation results of the BNDCAC-FIGARCH model in DAX 40

Parameter	Mean	Std	2.5%	25%	50%	75%	97.5%
ν	3.4139	1.1985	2.0695	2.5136	3.0106	4.1067	6.3688
ω	0.7321	0.3617	0.1758	0.4661	0.6941	0.9969	1.5477
ϕ	0.2375	0.1498	0.0111	0.0896	0.2595	0.3539	0.4899
d	0.5594	0.2520	0.0496	0.4125	0.5546	0.7590	0.9770
β	0.5128	0.3166	0.0037	0.2377	0.5508	0.8129	0.9747
γ	0.5163	0.5125	0.0006	0.0508	0.3380	0.9679	1.6219
θ_1	0.0486	0.0422	0.0013	0.0191	0.0337	0.0694	0.1541
θ_2	0.8702	0.0469	0.8029	0.8301	0.8620	0.9030	0.9618

Table 4 Out-of-sample performance of different estimators in DAX 40

Model	AV (%)	SD (%)	IR	SR
DCC	9.1868	16.5833	0.5540	0.4062
DCAC-GARCH	9.7245	16.7182	0.5817	0.4351
DCAC-FIGARCH	10.3219	17.0126	0.6067	0.4627
BNDCAC-FIGARCH	14.3576	22.2389	0.6456	0.5354

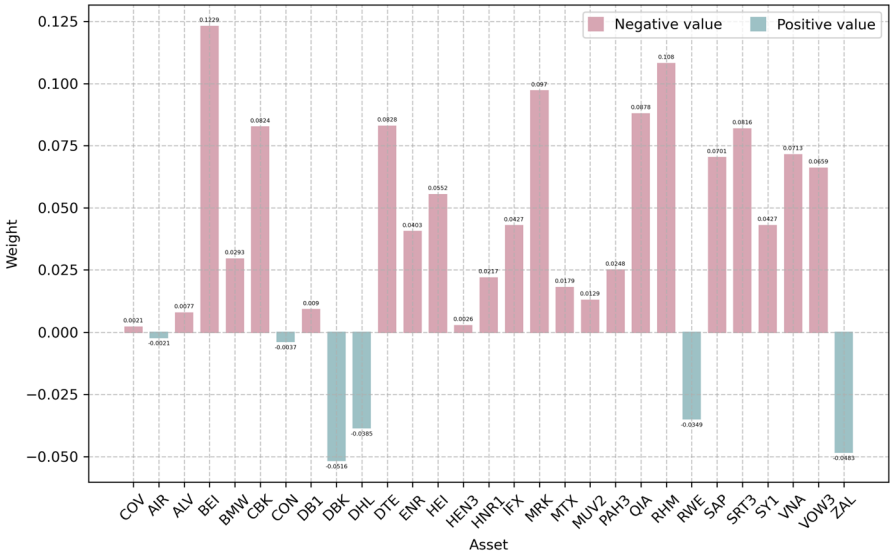

Fig. 10 Out-of-sample asset weights based on the BNDCAC-FIGARCH model in DAX 40

tionally, the low standard deviations of parameter estimates, combined with trace plot observations, validate the accuracy and effectiveness of the estimation results.

Following the aforementioned analysis of the model parameter estimation, this study further investigates the portfolio construction performance and practical application value of various models in DAX 40. Table 4 systematically summarizes the results of indicators in DAX 40 using different estimators, while Figs. 10 and 11 detail the dynamic evolution of asset allocation weights and out-of-sample returns for the portfolio strategy based on the BNDCAC-FIGARCH model.

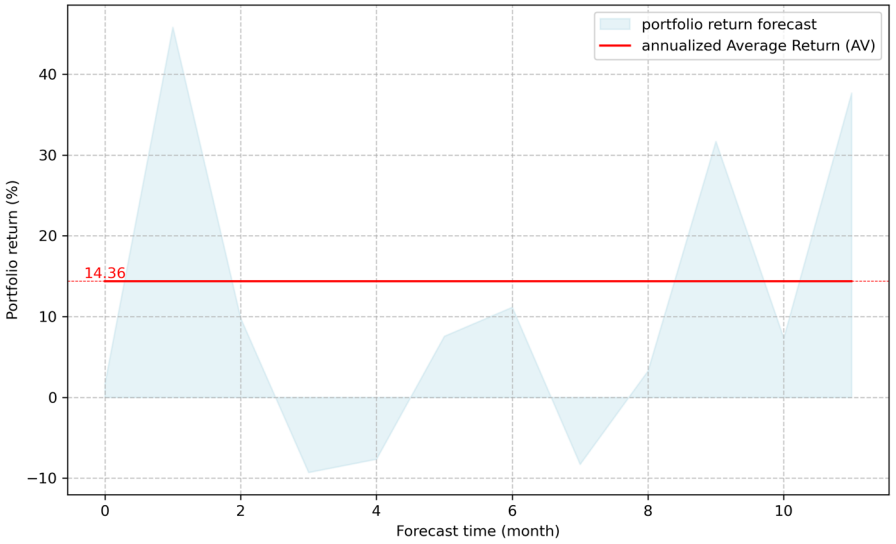

Fig. 11 Out-of-sample portfolio return based on the BNDCAC-FIGARCH model in DAX 40

Empirical results demonstrate that the BNDCAC-FIGARCH model exhibits significant advantages in financial markets like DAX 40 characterized by high kurtosis and non-normal distributions. The model not only achieves superior portfolio returns but also generates substantial excess returns, with AV reaching 14.36%, accompanied by IR and SR of 0.65 and 0.54 respectively. Although return enhancement inevitably accompanies increased portfolio risk, the model achieves effective risk-return balance through portfolio optimization. These findings align with the recent global financial context of intensified market volatility and heightened correlations among risk assets, indicating that the BNDCAC-FIGARCH model better captures asset return characteristics under extreme market fluctuations, thereby providing robust decision support for asset allocation in high-volatility environments.

Figure 12 presents the out-of-sample covariance prediction between the first and second constituent stocks of DAX 40 using the BNDCAC-FIGARCH model. The study replicates volatility patterns from 2017 to 2023, with a dedicated one-year out-of-sample forecasting window (252 trading days, equivalent to 12 trading months). The modeling period encompasses both the high-volatility phase of the Corona Virus Disease 2019 (COVID-19) pandemic, crude oil price collapse, and interventions of the Federal Reserve bank (2020), as well as the reduced-volatility period of economic recovery policies and the supply management led by the Organization of the Petroleum Exporting Countries (2023-2024). Empirical evidence confirms the model's precision in tracking dynamic covariance matrix evolution, particularly demonstrating the enhanced predictive capability during the extreme market turbulence.

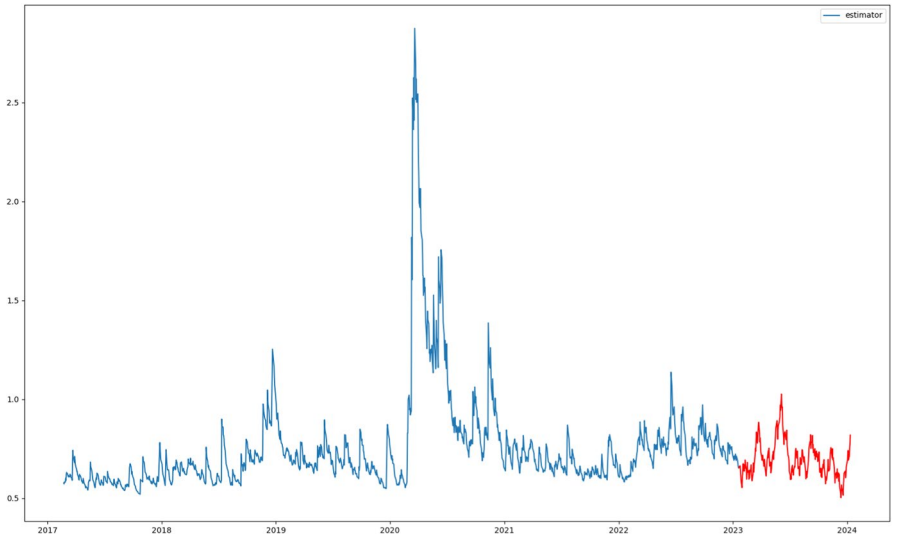

Fig. 12 Out-of-sample covariance estimation based on the BNDCAC-FIGARCH model in DAX 40

4.3.2 FTSE 100

For FTSE 100, Fig. 13 presents the posterior marginal distributions and parameter correlations estimated by the BNDCAC-FIGARCH model, with the corresponding sampling trace plots shown in Fig. 14.

From Fig. 13, the results reveal that the shape parameter ν of the distribution does not exhibit significant covariation patterns with other parameters, as evidenced by the absence of tightly clustered closed regions in their density contours while the overall image forms the rectangular regions parallel to the coordinate axes. Additionally, the graphical distribution between correlation parameters θ_1 and θ_2 manifests as a trapezoidal region concentrated near the coordinate axes, indicating a nonlinear dependence between them. Compared to the distinct triangular region observed in DAX 40, this trapezoidal distribution pattern reflects heterogeneity in parameter spaces across different market environments. In addition, from Fig. 14, under this sampling scheme, all parameters collectively tend toward the overall stationarity, validating the effectiveness of parameter estimation.

A comparison between the posterior and prior distributions of the parameters is illustrated in Fig. 15. It can be observed that the probability density functions of the posterior distributions for parameters β, ϕ, and d exhibit flatter shapes compared to their prior distributions, with significantly widened confidence intervals. This indicates heightened uncertainty in parameter estimation within real financial markets, as well as stronger nonlinear dynamics in the FTSE 100 market under extreme event shocks. For instance, during the pandemic period, markets were subjected to multiple heterogeneous shocks–including government policies, vaccine developments, and the pace of global economic recovery–which amplified the uncertainty in estimating these parameters in the model. On the other hand, the posterior distributions of correlation parameters θ_1 and θ_2 display more pronounced sharper peaks and heavier tails,

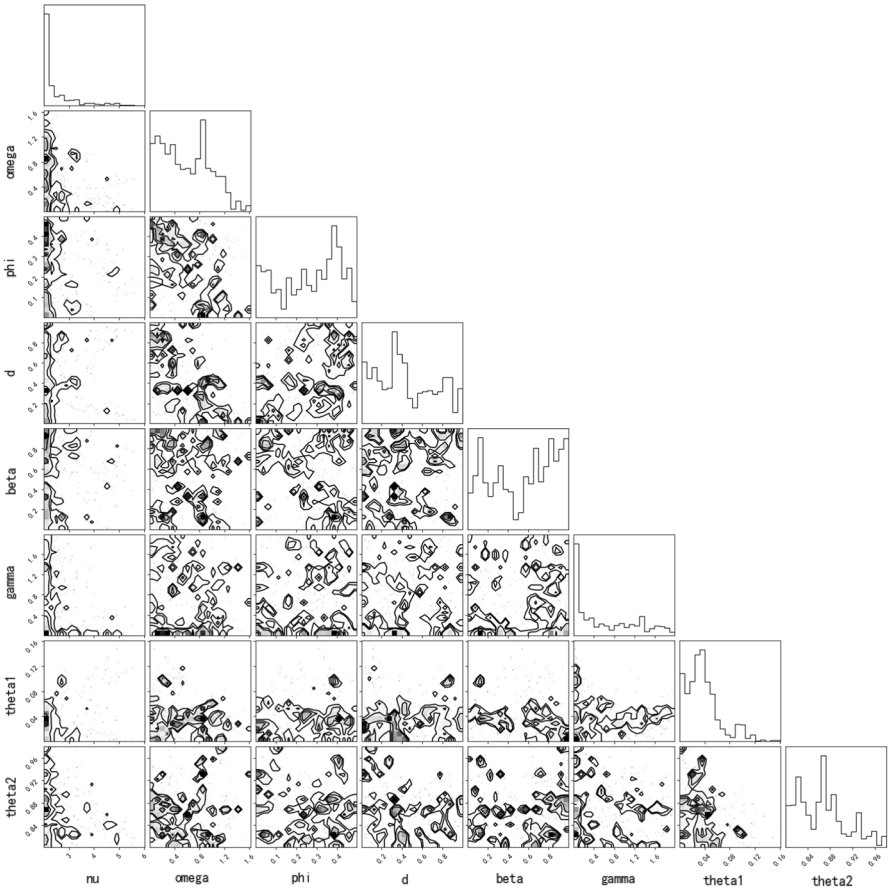

Fig. 13 The parameter marginal distribution and corner diagram in FTSE 100

with higher peak values relative to those observed in DAX 40. The statistical essence of this phenomenon can be attributed to the asymmetric amplification effects of financial market volatility under pandemic-driven shocks. In practical terms, the extreme market turbulence during the pandemic led to datasets exhibiting more prominent peakedness, while investors' heightened reliance on historical information further reinforced this peaked structure. Furthermore, structural analysis of the parameter space reveals that differences between parameters in the corner plots underscore how correlation parameters in financial markets are more susceptible to the influence of return characteristics. Consequently, the high kurtosis and heavy-tailed features of θ_1 and θ_2 not only reflect the statistical properties of the data itself but also present the environmental characteristics of financial markets.

Table 5 summarizes the parameter estimation results of the BNDCAC-FIGARCH model in FTSE 100. Specifically, the ν values for all assets exceed 2, indicating pronounced heavy-tailed behavior in the dataset. This reflects the heightened frequency of extreme events in financial markets, exemplified by the substantial socioeconomic impacts of the COVID-19 pandemic in 2020 and the formal Brexit implementation

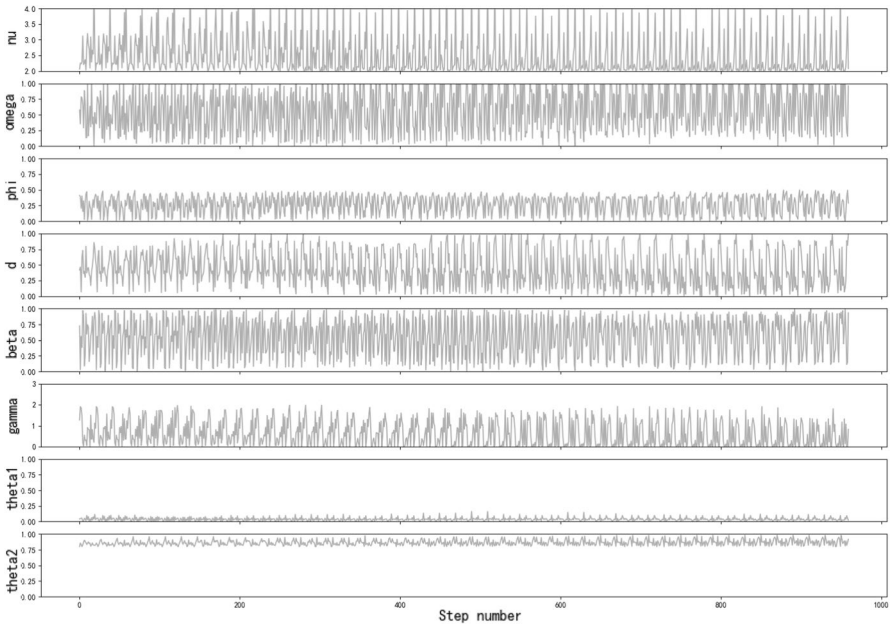

Fig. 14 The parameter trace in FTSE 100

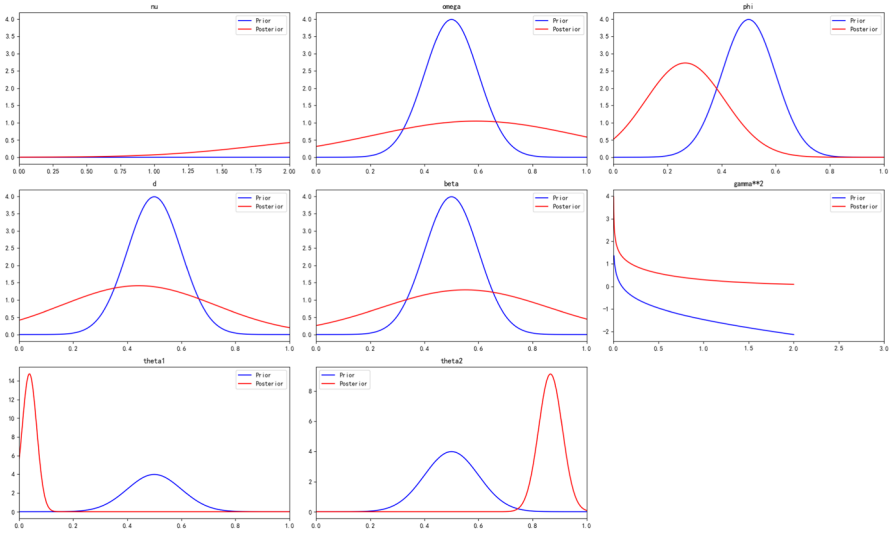

Fig. 15 The posterior distribution compared with the prior distribution in FTSE 100

in the UK during the same year. In addition, the combined average of correlation parameters $\theta_1 + \theta_2$ reaches 0.90, demonstrating significant persistence effects of historical data in risk forecasting. This elevated parameter combination reveals that historical market volatility characteristics carry substantial weight in future risk pre-

Table 5 Parameter estimation results of the BNDCAC-FIGARCH model in FTSE 100

Parameter	Mean	Std	2.5%	25%	50%	75%	97.5%
ν	2.5009	0.7494	2.0044	2.0303	2.1335	2.7116	4.8549
ω	0.5901	0.3807	0.0348	0.2465	0.5528	0.8755	1.2964
ϕ	0.2656	0.1460	0.0080	0.1428	0.2986	0.3892	0.4660
d	0.4420	0.2824	0.0305	0.2058	0.3922	0.6798	0.9790
β	0.5511	0.3088	0.0462	0.2701	0.6346	0.8251	0.9761
γ	0.6203	0.6075	0.0014	0.0414	0.3901	1.1398	1.8269
θ_1	0.0384	0.0270	0.0034	0.0215	0.0341	0.0487	0.1045
θ_2	0.8662	0.0437	0.8035	0.8273	0.8658	0.8877	0.9592

Table 6 Out-of-sample performance of different estimators in FTSE 100

Model	AV (%)	SD (%)	IR	SR
DCC	10.6877	9.7715	1.0938	0.6216
DCAC-GARCH	10.0376	10.7992	0.9295	0.5023
DCAC-FIGARCH	10.5833	10.4217	1.0155	0.5728
BNDCAC-FIGARCH	10.1526	7.5608	1.3428	0.7326

dictions, reflecting persistent interactions between investor behavioral patterns and market fluctuations in price formation. Lastly, the standard deviations of all parameter estimates are notably lower than their mean values, indicating high precision and stability in parameter estimation. This low-dispersion parameter distribution suggests minimal sampling estimation bias, thereby ensuring model reliability. In the post-pandemic era, while macroeconomic conditions show recovery trends, the persistent presence of asymmetric risks and exogenous shocks underscores the necessity of establishing the BNDCAC-FIGARCH model. The aforementioned parameter estimation results substantiate this conclusion.

Following the aforementioned analysis of the model parameter estimation, our focus now shifts to the portfolio optimization performance of the model in the FTSE 100 market. Table 6 summarizes the results of indicators in FTSE 100 using different estimators, while Figs. 16 and 17 illustrate the asset weight allocations and out-of-sample portfolio return evolution of the BNDCAC-FIGARCH model in FTSE 100.

In the FTSE 100 market characterized by extreme kurtosis and non-normal distributions, the BNDCAC-FIGARCH model achieves superior portfolio returns and excess returns while significantly reducing portfolio risk. The model delivers an AV of 10.15%, with IR and SR in excess returns reaching 1.34 and 0.73, respectively, while maintaining a portfolio risk SD of only 7.56%.

Specifically, the BNDCAC-FIGARCH model demonstrates additional risk reduction compared to DAX 40, primarily attributable to the higher kurtosis in FTSE 100. Elevated kurtosis indicates a higher frequency of extreme market shocks, particularly post-2020, where the market turbulence induced by the COVID-19 pandemic and the Brexit's persistent impacts on the British stock market have created the sustained volatility. Traditional models often fail to adequately capture these shocks, whereas the BNDCAC-FIGARCH model effectively mitigates portfolio risk through enhanced covariance matrix prediction accuracy by incorporating non-normal infor-

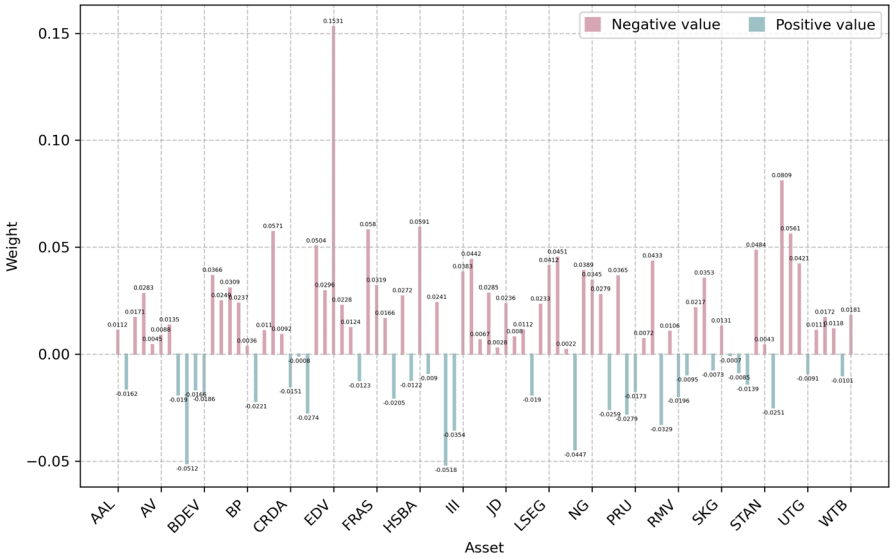

Fig. 16 Out-of-sample asset weights based on the BNDCAC-FIGARCH model in FTSE 100

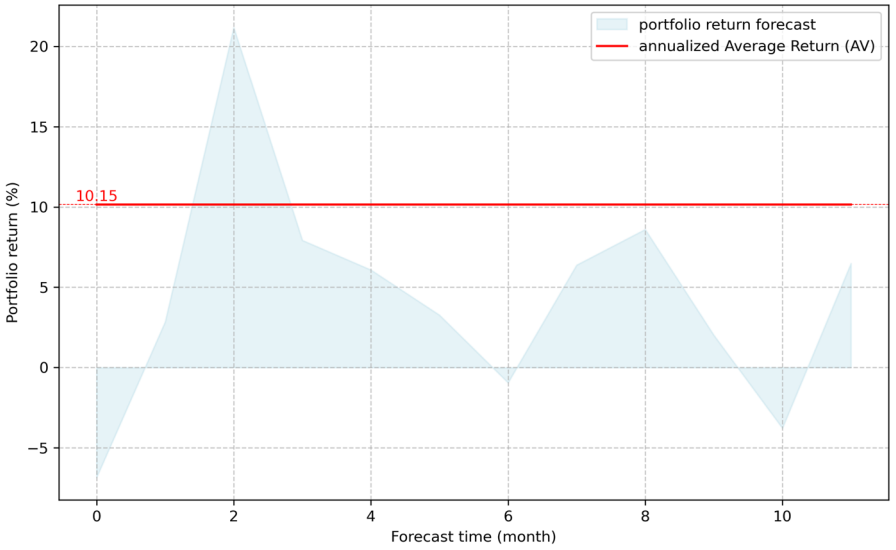

Fig. 17 Out-of-sample portfolio return based on the BNDCAC-FIGARCH model in FTSE 100

mation. This capability enables more precise identification and pricing in high-kurtosis markets.

The results presented in Figs. 16 and 17 further validate the practical effectiveness of the BNDCAC-FIGARCH model. Combined with the numerical outcomes in Table 6, it is evident that the BNDCAC-FIGARCH model achieves a Pareto improvement in risk-return trade-offs across different market cycles. Specifically, the

model enhances portfolio returns while simultaneously reducing the risk metric SD, demonstrating the critical role of precise covariance matrix estimation in effective risk diversification.

Figure 18 illustrates the out-of-sample predictions for the covariance between the first and second component stocks in FTSE 100 using the BNDCAC-FIGARCH model, with the out-of-sample period spanning one year. During 2020, FTSE 100 exhibited significantly higher volatility compared to DAX 40, likely attributable to multiple shocks impacting the British economy, including uncertainties stemming from the conclusion of the Brexit transition period. In the out-of-sample period (2023–2024), although overall market conditions stabilized, a pronounced negative volatility spike emerged in mid-2023. This phenomenon may be linked to the confluence of factors such as macroeconomic policy adjustments, intensified geopolitical risks (e.g., prolonged Russia-Ukraine conflict), and heightened market risk aversion, which collectively exacerbated equity price declines and amplified negative volatility. Additionally, technical corrections further amplified downward pressures, particularly following the breach of key support levels after prior upward trends.

4.3.3 SSE 50

For SSE 50, Fig. 19 presents the posterior marginal distributions and parameter correlations estimated by the BNDCAC-FIGARCH model, with the corresponding sampling trace plots shown in Fig. 20.

From Fig. 19, the results reveal no significant correlations between parameters ν and ω and other parameters, evidenced by the approximately parallel linear alignment of contour lines along coordinate axes. Further analysis indicates that the joint distribution of correlation parameters θ_1 and θ_2 exhibits a typical tail dependence structure, with the closed regions resembling the asymmetric triangular shapes,

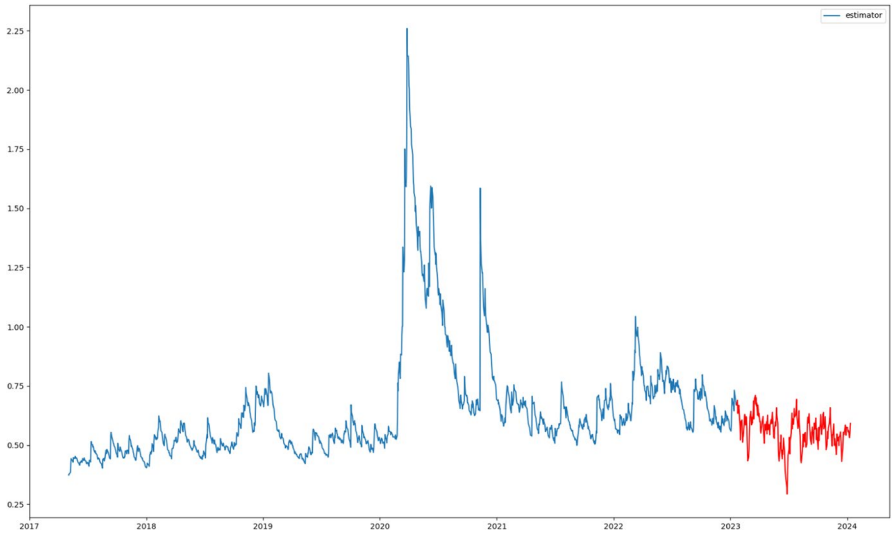

Fig. 18 Out-of-sample covariance estimation based on the BNDCAC-FIGARCH model in FTSE 100

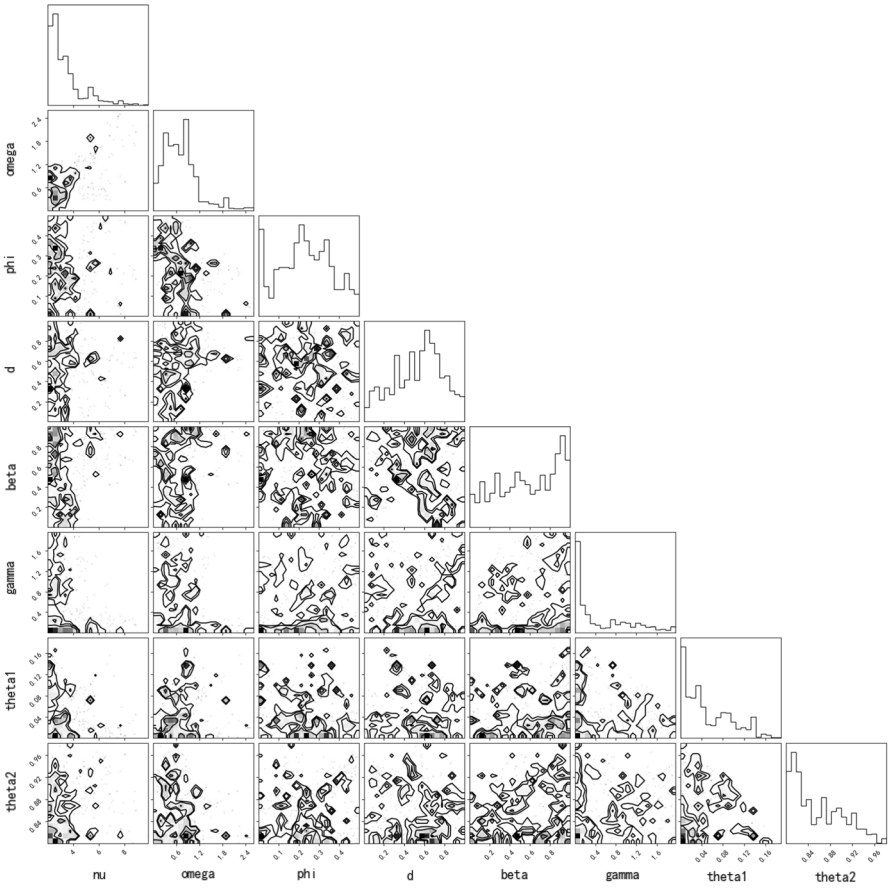

Fig. 19 The parameter marginal distribution and corner diagram in SSE 50

thereby revealing a nonlinear coupling relationship between them. Notably, while these closed regions share similarities with those observed in FTSE 100, SSE 50 demonstrates more pronounced dispersion characteristics, manifested as independent and relatively scattered closed regions. This demonstrates the BNDCAC-FIGARCH model's ability to capture distinct market microstructures across different financial environments. In addition, Fig. 20 displays the parameter sampling trace. As shown, all parameters ultimately stabilize over time, confirming the validity of the model parameter estimation.

A comparative analysis of posterior and prior distributions for model parameters is presented in Fig. 21. The posterior distributions of parameters β, ϕ, and d exhibit lower peak densities and broader dispersion ranges compared to their prior distributions. In contrast, the posterior distributions of θ_1 and θ_2 demonstrate sharper peaks and heavier tails, a pattern consistent with observations in other financial markets. Notably, the elevated posterior estimates of parameter γ in SSE 50 reflect more pronounced asymmetric effects in this market. This asymmetry likely stems from regulatory interventions and investor behavioral biases specific to China's evolving equity

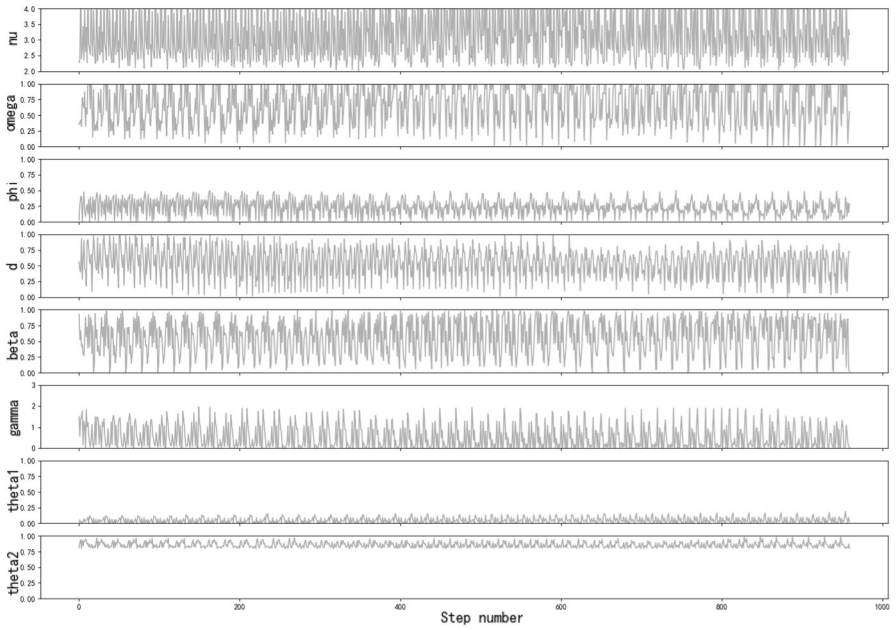

Fig. 20 The parameter trace in SSE 50

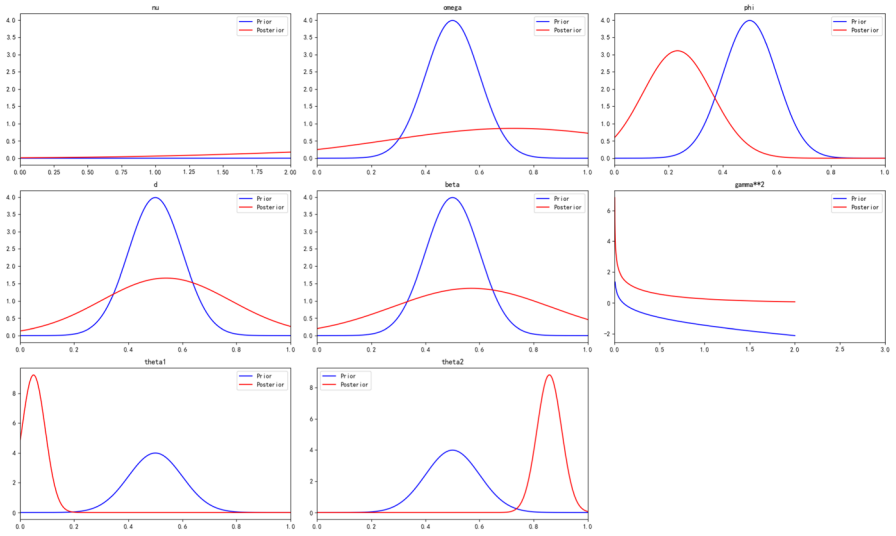

Fig. 21 The posterior distribution compared with the prior distribution in SSE 50

market structure, where policy-driven volatility suppression coexists with retail investor-driven momentum trading.

Table 7 summarizes the estimation results of the BNDCAC-FIGARCH model in SSE 50. The parameter estimates reveal that the minimum value of parameter d

Table 7 Parameter estimation results of the BNDCAC-FIGARCH model in SSE 50

Parameter	Mean	Std	2.5%	25%	50%	75%	97.5%
ν	3.3794	1.3301	2.1218	2.4534	2.9117	3.8213	7.4177
ω	0.7247	0.4609	0.0557	0.3807	0.6622	0.9125	1.9226
ϕ	0.2331	0.1282	0.0133	0.1383	0.2289	0.3305	0.4703
d	0.5395	0.2398	0.0675	0.3509	0.5770	0.7143	0.9620
β	0.5703	0.2918	0.0490	0.3063	0.5825	0.8533	0.9795
γ	0.5206	0.5648	0.0017	0.0420	0.2411	0.9564	1.8446
θ_1	0.0499	0.0432	0.0012	0.0128	0.0349	0.0811	0.1395
θ_2	0.8579	0.0453	0.8020	0.8182	0.8441	0.8929	0.9548

Table 8 Out-of-sample performance of different estimators in SSE 50

Model	AV (%)	SD (%)	IR	SR
DCC	-1.2381	20.5150	-0.0603	-0.1781
DCAC-GARCH	9.6774	23.7594	0.4073	0.3056
DCAC-FIGARCH	9.4033	23.5277	0.3997	0.2970
BNDCAC-FIGARCH	15.2071	33.3580	0.4559	0.3835

exceeds 0.5, indicating the long-term memory characteristics. Such long memory properties are particularly critical in financial markets, especially in emerging markets like China, where volatility persistence is amplified by factors including policy shifts, evolving market structures, and heterogeneous investor behavior. For instance, during the COVID-19 pandemic in 2020, the Chinese government implemented a series of economic stimulus measures to stabilize markets. The prolonged impact of these policies has engendered observable long memory patterns in SSE 50. The estimated values of parameter ν universally satisfy the constraint $\nu > 2$, statistically guaranteeing the positive definiteness of high-dimensional covariance matrices. This result simultaneously confirms the leptokurtic and heavy-tailed characteristics of return series under non-normal distributions. Such statistical properties underscore the limitations of traditional normality assumptions in risk measurement during extreme market conditions. Furthermore, the combined average of correlation parameters θ_1 and θ_2 reaches 0.90, robustly validating the historical persistence embedded in the volatility process. This high parameter magnitude highlights the dominant role of past volatility shocks in shaping future risk dynamics, aligning with the behavioral patterns of market participants who exhibit adaptive responses to prolonged policy and macroeconomic uncertainties.

Following the aforementioned analysis of the model parameter estimation, this study further investigates the portfolio construction performance and practical application value of various models in SSE 50. Table 8 summarizes the results of indicators in SSE 50 with different estimators, while Figs. 22 to 23 illustrate the asset weight allocations and out-of-sample portfolio return derived from the BNDCAC-FIGARCH model.

Empirical comparisons demonstrate that portfolios constructed with the BNDCAC-FIGARCH model achieve significantly higher risk-adjusted returns (quantified by SR) during the out-of-sample testing period. This performance is primarily driven by a substantial increase in portfolio returns that offsets the elevated risk exposure, as

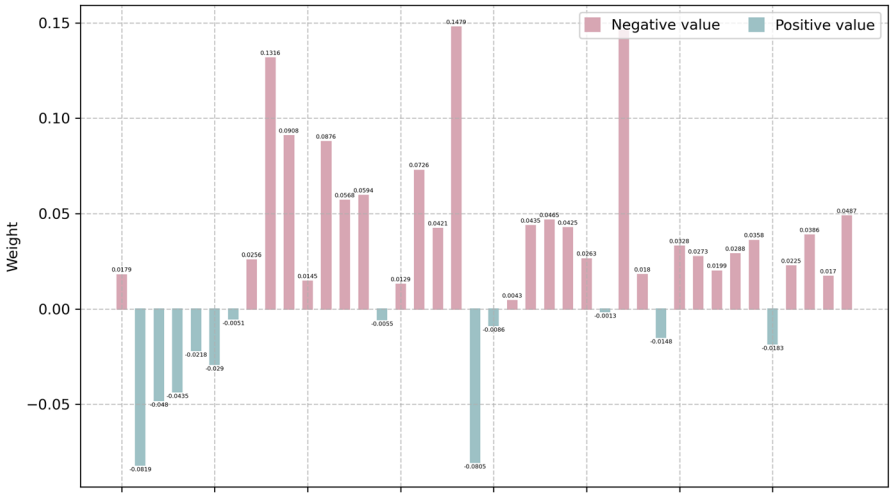

Fig. 22 Out-of-sample asset weights based on the BNDCAC-FIGARCH model in SSE 50

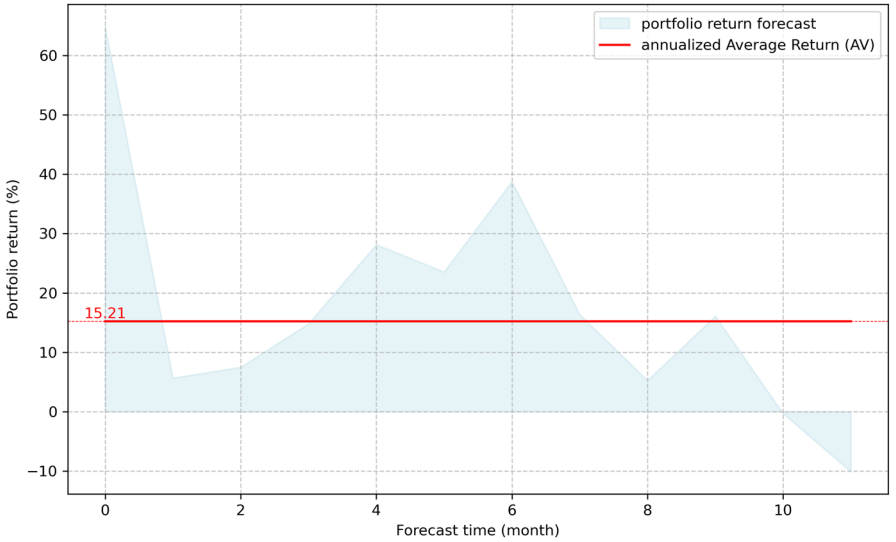

Fig. 23 Out-of-sample portfolio return based on the BNDCAC-FIGARCH model in SSE 50

evidenced by the pronounced temporal divergence in return dynamics across different market phases. Specifically, the results in Figs. 22 and 23 reveal the model's asymmetric risk compensation capability during extreme market volatility. And the framework dynamically adjusts asset weights to amplify return capture in bullish regimes while mitigating drawdowns in bearish phases, thereby enhancing overall profitability. The time-varying return patterns further demonstrate the BNDCAC-FIGARCH model's enhanced adaptability to wild fluctuation in SSE 50, where conventional mean-variance strategies frequently struggle to optimize risk-return tradeoffs. This

superior performance originates from the model's effective integration of two critical features: long-term memory and non-normal distribution characteristics.

Figure 24 presents the out-of-sample forecasts for the covariance between the first and second constituent stocks in SSE 50 based on the BNDCAC-FIGARCH model, covering a one-year out-of-sample period. Compared to other markets, SSE 50 exhibited relatively muted volatility during 2020. This stability likely stemmed from the Chinese government's vigorous economic stimulus measures and stringent pandemic containment policies, which effectively stabilized financial markets while mitigating the impacts of the COVID-19 pandemic. Additionally, the market's relative insularity and unique domestic investor composition buffered against external shocks. However, the significant negative volatility emerged in the latter half of the 2024 forecast period, attributable to multiple interconnected factors. First, the global economic recovery decelerated amid rising inflationary pressures, prompting central banks to gradually exit accommodative monetary policies and initiate interest rate hikes. Such policy tightening directly increased corporate financing costs and suppressed investor risk appetite, particularly affecting large-cap indices like SSE 50 that are sensitive to macroeconomic shifts. Second, escalating geopolitical tensions, including the trade uncertainty between China and the United States and regional conflicts, amplified the market risk aversion. Third, corporate profitability faced dual pressures from rising operational costs and weakened demand in 2024, particularly in export-oriented and technology sectors within SSE 50. These combined forces constrained earnings growth and exerted downward pressure on equity valuations.

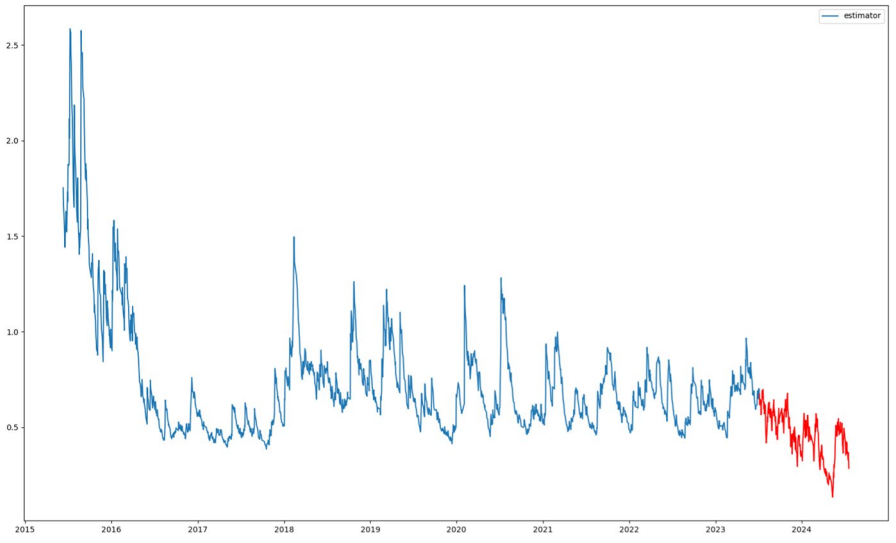

Fig. 24 Out-of-sample covariance estimation based on the BNDCAC-FIGARCH model in SSE 50

4.3.4 CSI 100

For CSI 100, Fig. 25 presents the posterior marginal distributions and parameter correlations estimated by the BNDCAC-FIGARCH model, with the corresponding sampling trace plots shown in Fig. 26.

From Fig. 25, the results show that most parameters are largely consistent with previous findings, thus requiring no redundant elaboration. Notably, the closed regions between correlation parameters θ_1 and θ_2 manifest as a horizontal trapezoidal shape, indicating a distinct nonlinear dependence compared to prior observations. This highlights the model's enhanced capability to capture non-normally distributed market characteristics. In addition, from Fig. 26, all parameters ultimately converge to stability, demonstrating the validity of parameter estimation.

Table 9 summarizes the parameter estimation results of the BNDCAC-FIGARCH model for CSI 100, with a comparative analysis of posterior and prior distributions presented in Fig. 27. Empirical results indicate that all ν values exceed 2, confirming the validity of the estimated covariance matrices. The asymmetric response parameter

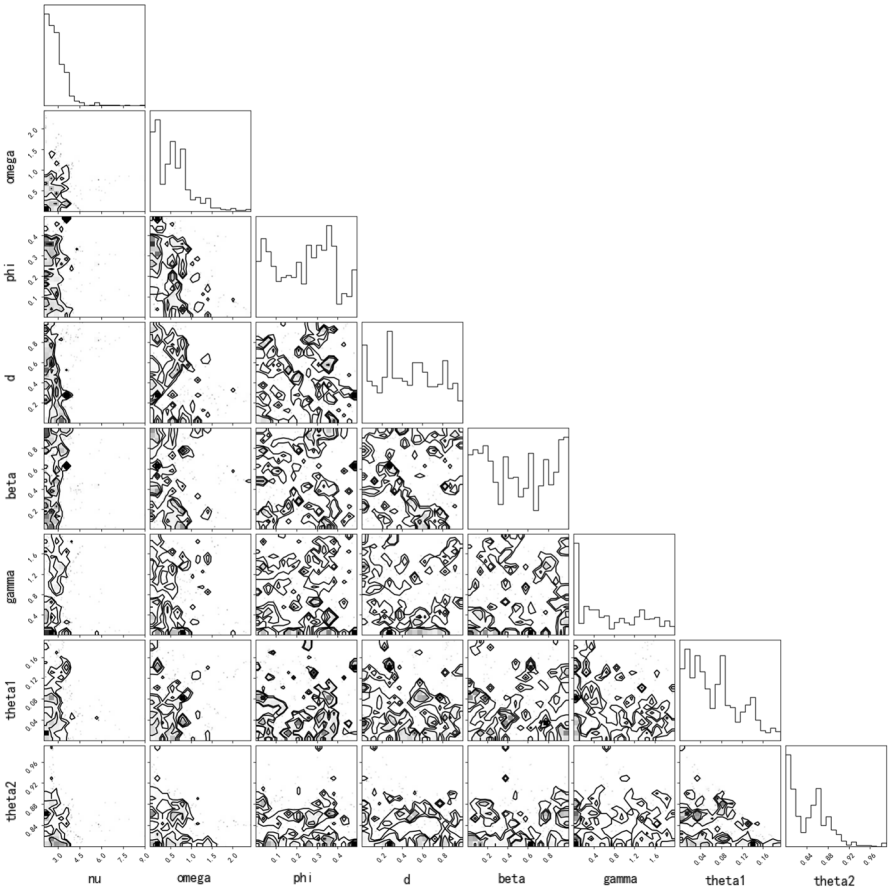

Fig. 25 The parameter marginal distribution and corner diagram in CSI 100

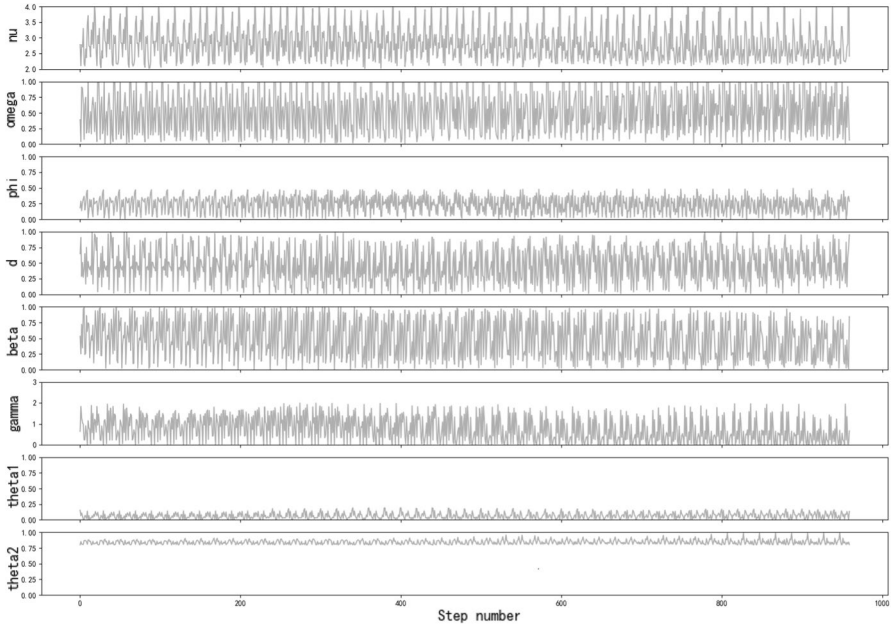

Fig. 26 The parameter trace in CSI 100

Table 9 Parameter estimation results of the BNDCAC-FIGARCH model in CSI 100

Parameter	Mean	Std	2.5%	25%	50%	75%	97.5%
ν	2.8699	0.7609	2.1083	2.3410	2.7183	3.1721	4.5739
ω	0.5514	0.4332	0.0296	0.1984	0.5214	0.7679	1.6373
ϕ	0.2338	0.1360	0.0165	0.1078	0.2570	0.3479	0.4686
d	0.4661	0.2795	0.0132	0.2553	0.4531	0.6982	0.9435
β	0.4962	0.3147	0.0244	0.1924	0.4793	0.7804	0.9846
γ	0.7421	0.6180	0.0017	0.1630	0.5985	1.3199	1.8635
θ_1	0.0673	0.0482	0.0022	0.0268	0.0579	0.0989	0.1738
θ_2	0.8441	0.0354	0.8011	0.8112	0.8423	0.8657	0.9247

γ for CSI 100 is significantly higher than that of SSE 50 and approaches 1, suggesting the weaker asymmetry in CSI 100. This phenomenon may arise from market capacity expansion, where hedging effects generated by asymmetric characteristics of certain constituent assets mitigate the overall market's asymmetric response intensity. The combined average of correlation parameters $\theta_1 + \theta_2$ reaches 0.91, underscoring the substantial influence of historical data on risk forecasting. Additionally, the low standard deviations of all parameter estimates corroborate the robustness of the BNDCAC-FIGARCH model specification within the Bayesian inference framework.

Following the aforementioned analysis of the model parameter estimation, this study further investigates the portfolio construction performance and practical application value of various models in CSI 100. Table 10 summarizes the results of indicators in CSI 100 with different estimators, while Figs. 28 to 29 illustrate the asset

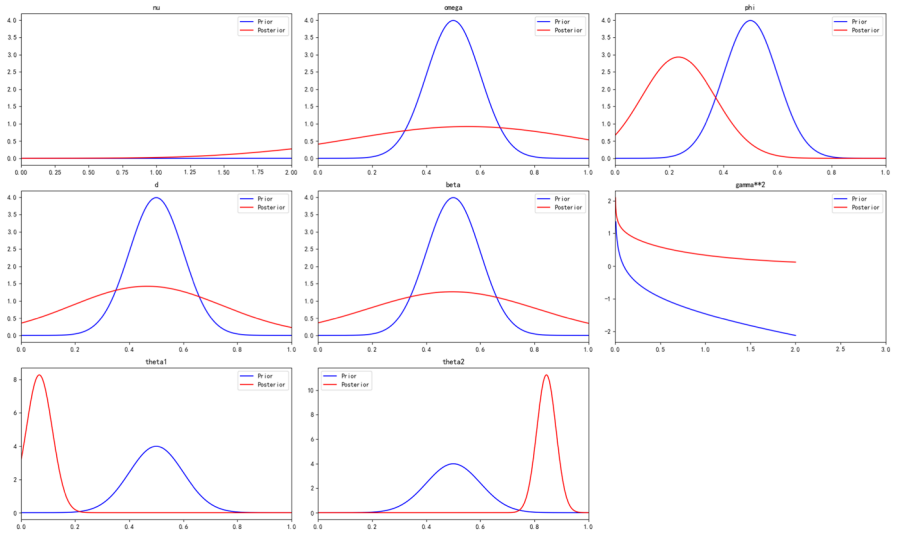

Fig. 27 The posterior distribution compared with the prior distribution in CSI 100

Table 10 Out-of-sample performance of different estimators in CSI 100

Model	AV (%)	SD (%)	IR	SR
DCC	-4.6688	23.5784	-0.1980	-0.3005
DCAC-GARCH	-2.7413	23.1728	-0.1183	-0.2225
DCAC-FIGARCH	4.9763	19.6788	0.2529	0.1301
BNDCAC-FIGARCH	10.4348	24.2268	0.4307	0.3310

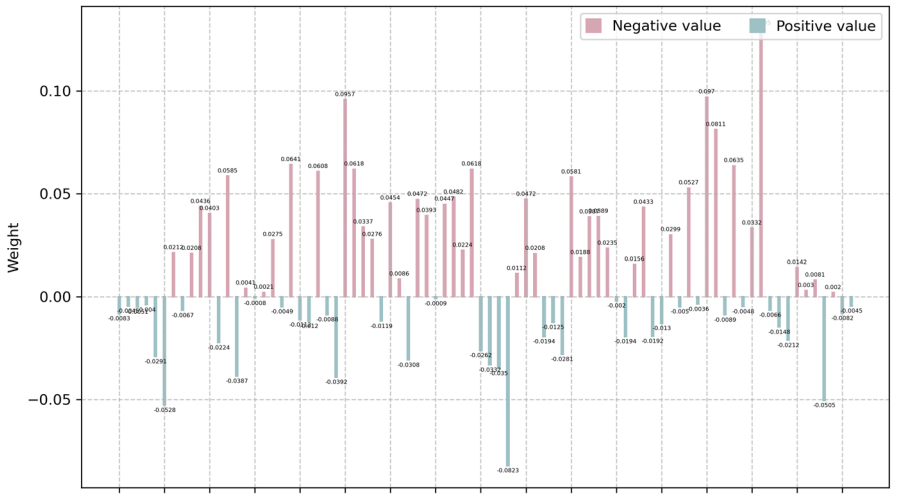

Fig. 28 Out-of-sample asset weights based on the BNDCAC-FIGARCH model in CSI 100

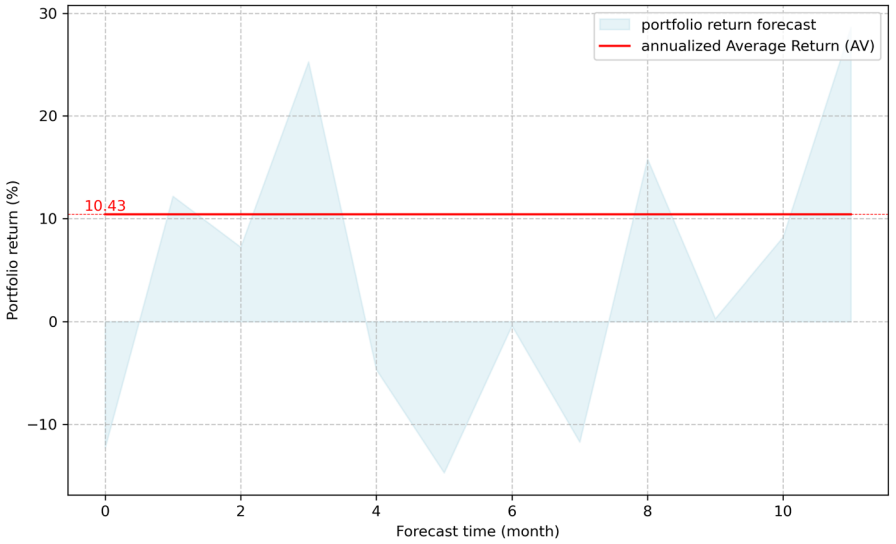

Fig. 29 Out-of-sample portfolio return based on the BNDCAC-FIGARCH model in CSI 100

weight allocations and out-of-sample portfolio return derived from the BNDCAC-FIGARCH model.

Empirical analysis demonstrates that the BNDCAC-FIGARCH model, which incorporates the long-term memory effects and non-normal distribution characteristics, consistently generates positive portfolio returns, whereas classical models exhibit negative return profiles. This return divergence reveals significant heterogeneity and non-normal distribution features in the financial market data. Specifically, in CSI 100 with kurtosis approximating normality, the BNDCAC-FIGARCH model still achieves higher portfolio returns, albeit with elevated portfolio risk accompanying the substantial increase in excess returns. The portfolio delivers AV of 10.43%, SD of 24.23%, and an improved SR of 0.33. This finding suggests that the BNDCAC-FIGARCH model should be applied with caution when analyzing near-normally distributed data. Consequently, investors need to carefully balance risk-return tradeoffs when implementing this framework.

Figure 30 presents the out-of-sample forecasts for the covariance between the first and second constituent stocks in CSI 100 based on the BNDCAC-FIGARCH model, covering a one-year out-of-sample period. The results reveal persistent high volatility characteristics in both historical and forecast periods. This volatility anomaly stems from three endogenous drivers: First, the dynamic contest between emerging and traditional industries during China's economic structural transformation has created structural mismatches in market expectations (manifested as discrepancies between capital risk appetite and actual asset risks, and misalignments between asset prices and intrinsic risks). Second, counter-cyclical adjustments in monetary and fiscal policies have triggered liquidity stratification, particularly through the combined effects of the moderately accommodative monetary policy and proactive fiscal policy, intensifying short-term fluctuations in capital pricing mechanisms. Third, behavioral distortions among market participants under the reform of Initial Public Offering

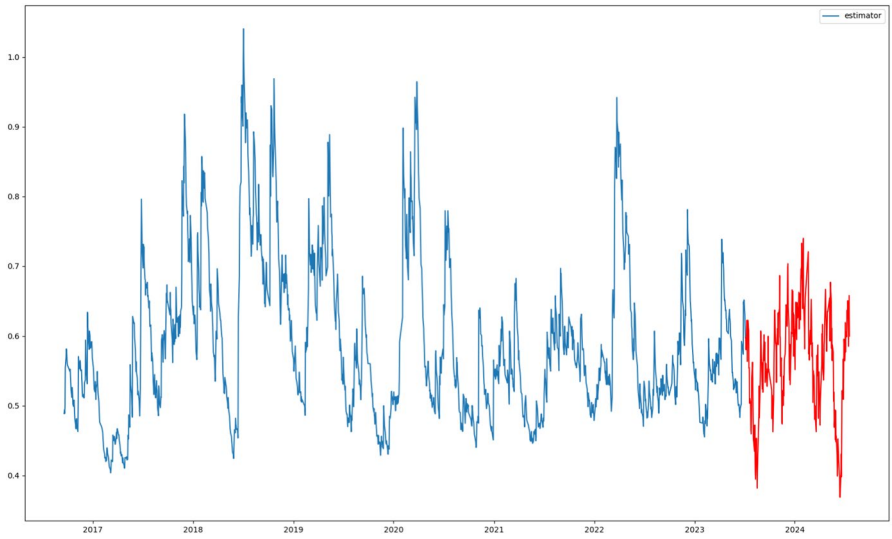

Fig. 30 Out-of-sample covariance estimation based on the BNDCAC-FIGARCH model in CSI 100

based on registration, particularly the herding behavior amplified by the excessive proportion of retail investors, have magnified time-lag impacts in information transmission. Additionally, shifts in the global macroeconomic environment have further exacerbated market volatility.

5 Conclusion

In this paper, we have presented the BNDCAC-FIGARCH model by introducing the asymmetric parameter and student's t-distribution into the DCAC-FIGARCH model. In the simulation experiment, we have set the innovation to satisfy the student's t-distribution and repeat the experiment 20 times to calculate the average value. The results show that under the overall correlation coefficient path of sine and ramp shapes, the BNDCAC-FIGARCH model can obtain a more accurate estimate based on the student's t-distribution, proving the effectiveness and stability of the model. Finally, experiments using several historical stock indices are conducted, including DAX 40, FTSE 100, SSE 50 and CSI 100. The out-of-sample results show that the BNDCAC-FIGARCH model effectively reduces the parameter uncertainty and improves portfolio returns. Moreover, the parameter estimation results demonstrate the robust performance of the BNDCAC-FIGARCH model in real-world situations. Meanwhile, in the modeling and forecasting of the stock market volatility, it is found that CSI 100 with the weaker asymmetry differs from other indices. One possible reason is that the more liquid market better reflects the improvement in economic conditions brought about by national policies in recent years.

Future research may focus on two directions. First, a more comprehensive model comparison could be conducted using advanced Bayesian assessment tools such as the log pseudo marginal likelihood and the widely applicable information criterion.

Second, integrating machine learning techniques might refine the prior information in the BNDCAC-FIGARCH model, further mitigating parameter uncertainty.

Author contributions Zhangshuang Sun: Conceptualization, Methodology, Software, Validation, Formal analysis, Investigation, Resources, Data curation, Writing - original draft, Writing - review & editing, Visualization. Qian Li: Writing - review & editing, Visualization. Haixiang Lin: Software, Writing - review & editing. Guoqiang Wang: Writing - review & editing, Methodology, Investigation, Funding acquisition, Project administration, Conceptualization.

Funding This work was funded by the National Natural Science Foundation of China (Grants Nos. 11971302, 12171307).

Data availability Data on constituent stocks of stock indices were collected from the Google Finance and the Tushare platform, available at https://www.google.com/finance and https://www.tushare.pro respectively.

Declarations

Conflicts of Interest The authors declare they have no financial interests.

Ethical Approval This article does not contain any studies with human participants or animals performed by any of the authors.

Consent to Participate Consent for publication was obtained from the participants.

References

Anyah, A. D., Ahmed, A., Rasheed, B. A., et al. (2025). Comparative analysis between garch and figarch models for the prediction of volatility in financial time series models. *International Journal of Innovative Mathematics, Statistics & Energy Policies, 13*(3), 99–112. https://doi.org/10.5281/zenodo.16542117

Bauwens, L., De Backer, B., & Dufays, A. (2014). A bayesian method of change-point estimation with recurrent regimes: Application to garch models. *Journal of Empirical Finance, 29*, 207–229. https://doi.org/10.1016/j.jempfin.2014.06.008

Belkhouja, M., & Boutahary, M. (2011). Modeling volatility with time-varying figarch models. *Economic Modelling, 28*(3), 1106–1116. https://doi.org/10.1016/j.econmod.2010.11.017

Bollerslev, T. (1986). Generalized autoregressive conditional heteroskedasticity. *Journal of Econometrics, 31*(3), 307–327. https://doi.org/10.1016/0304-4076(86)90063-1

Brooks, S. P., Giudici, P., & Philippe, A. (2003). Nonparametric convergence assessment for mcmc model selection. *Journal of Computational and Graphical Statistics, 12*(1), 1–22. https://doi.org/10.1198/1061860031347

Cai, T. T., Ren, Z., & Zhou, H. H. (2016). Estimating structured high-dimensional covariance and precision matrices: Optimal rates and adaptive estimation. *Electronic Journal of Statistics, 10*, 1–59. https://doi.org/10.1214/15-EJS1081

Cai, X., Teo, K. L., Yang, X., et al. (2000). Portfolio optimization under a minimax rule. *Management Science, 46*(7), 957–972. https://doi.org/10.1287/mnsc.46.7.957.12039

De Nard, G., Ledoit, O., & Wolf, M. (2021). Factor models for portfolio selection in large dimensions: The good, the better and the ugly. *Journal of Financial Econometrics, 19*(2), 236–257. https://doi.org/10.5167/uzh-151986

De Nard, G., Engle, R., Ledoit, O., et al. (2022). Large dynamic covariance matrices: Enhancements based on intraday data. *Journal of Banking & Finance, 138*, Article 106426. https://doi.org/10.1016/j.jbankfin.2022.106426

Engel, J., Buydens, L., & Blanchet, L. (2017). An overview of large-dimensional covariance and precision matrix estimators with applications in chemometrics. *Journal of Chemometrics, 31*(4), Article e2880. https://doi.org/10.1016/j.ecosta.2021.04.008

Engle, R. (2002). Dynamic conditional correlation: A simple class of multivariate generalized autoregressive conditional heteroskedasticity models. *Journal of Business & Economic Statistics, 20*(3), 339–350. https://doi.org/10.1198/073500102288618487

Engle, R., & Colacito, R. (2006). Testing and valuing dynamic correlations for asset allocation. *Journal of Business & Economic Statistics, 24*(2), 238–253. https://doi.org/10.1198/073500106000000017

Engle, R., Ledoit, O., & Wolf, M. (2019). Large dynamic covariance matrices. *Journal of Business & Economic Statistics, 37*(2), 363–375. https://doi.org/10.1080/07350015.2017.1345683

Fernández, C., & Steel, M. F. (1998). On bayesian modeling of fat tails and skewness. *Journal of the American Statistical Association, 93*(441), 359–371. https://doi.org/10.1080/01621459.1998.10474117

Fioruci, J. A., Ehlers, R. S., & Andrade Filho, M. G. (2014). Bayesian multivariate garch models with dynamic correlations and asymmetric error distributions. *Journal of Applied Statistics, 41*(2), 320–331. https://doi.org/10.1080/02664763.2013.839635

Goldman, E. (2023). Uncertainty in systemic risks rankings: Bayesian and frequentist analysis. *Finance Research Letters, 56*, Article 104028. https://doi.org/10.1016/j.frl.2023.104028

Jarjour, R., & Chan, K. S. (2020). Dynamic conditional angular correlation. *Journal of Econometrics, 216*(1), 137–150. https://doi.org/10.1016/j.jeconom.2020.01.010

Li, B., Shu, Y., Sun, Y., et al. (2021). An optimistic value-variance-entropy model of uncertain portfolio optimization problem under different risk preferences. *Soft Computing, 25*(5), 3993–4001. https://doi.org/10.1007/s00500-020-05423-4

Li, B., Sun, Y., & Teo, K. L. (2022). An analytic solution for multi-period uncertain portfolio selection problem. *Fuzzy Optimization and Decision Making, 21*(2), 319–333. https://doi.org/10.1007/s10700-021-09367-8

Li, D. (2024). Estimation of large dynamic covariance matrices: A selective review. *Econometrics and Statistics, 29*, 16–30. https://doi.org/10.1002/cem.2880

Li, P., & Xiao, Y. (2018). An efficient algorithm for sparse inverse covariance matrix estimation based on dual formulation. *Computational Statistics & Data Analysis, 128*, 292–307. https://doi.org/10.1016/j.csda.2018.07.011

Long, X., Su, L., & Ullah, A. (2011). Estimation and forecasting of dynamic conditional covariance: A semiparametric multivariate model. *Journal of Business & Economic Statistics, 29*(1), 109–125. https://doi.org/10.1198/jbes.2009.07057

Meng, R., Yang, F., & Kim, W. H. (2023). Dynamic covariance estimation via predictive wishart process with an application on brain connectivity estimation. *Computational Statistics & Data Analysis, 185*, Article 107763. https://doi.org/10.1016/j.csda.2023.107763

Nakajima, J., & Omori, Y. (2012). Stochastic volatility model with leverage and asymmetrically heavy-tailed error using gh skew student's t-distribution. *Computational Statistics & Data Analysis, 56*(11), 3690–3704. https://doi.org/10.1016/j.csda.2010.07.012

Nascimento, D., Xavier, C., Felipe, I.J.d.S., & Neto, F. L. (2019). Dynamic conditional correlation garch: A multivariate time series novel using a bayesian approach. Journal of Modern Applied Statistical Methods 18(1):2–17. https://doi.org/10.22237/jmasm/1556669220

Prass, T. S., Lopes, S. R., & Achcar, J. A. (2016). Mcmc bayesian estimation in fiegarch models. *Communications in Statistics-Simulation and Computation, 45*(9), 3238–3258. https://doi.org/10.1080/03610918.2014.932800

Sáfadi, T., Pereira, I. (2010). Bayesian analysis of fiaparch model: An application to sao paulo stock market. International Journal of Statistics and Economics 5(10):49–63. https://api.core.ac.uk/oai/oai:ria.ua.pt:10773/4426

Shiferaw, Y. A. (2019). Time-varying correlation between agricultural commodity and energy price dynamics with bayesian multivariate dcc-garch models. *Physica A: Statistical Mechanics and Its Applications, 526*, Article 120807. https://doi.org/10.1016/j.physa.2019.04.043

Sinharay, S. (2003). Assessing convergence of the markov chain monte carlo algorithms: A review. *ETS Research Report Series, 2003*(1), i–52. https://doi.org/10.1002/j.2333-8504.2003.tb01899.x

So, M.K., Liu, W.K., Chu, A.M. (2018). Bayesian shrinkage estimation of time-varying covariance matrices in financial time series. Advances in Decision Sciences 22(A):1–35. https://doi.org/10.47654/v22y2018i1p369-404

Sun, Z., Gao, X., Luo, K., et al. (2025). Enhancing high-dimensional dynamic conditional angular correlation model based on garch family models: Comparative performance analysis for portfolio optimization. *Finance Research Letters, 75*, Article 106808. https://doi.org/10.1016/j.frl.2025.106808

Tang, C., & Aruga, K. (2021). Relationships among the fossil fuel and financial markets during the covid-19 pandemic evidence from bayesian dcc-mgarch models. *Sustainability, 14*(1), 51. https://doi.org/10.3390/su14010051

Tukur, K. (2024). Time-varying correlation between seafood and meat index in the presence of ocean pollution shock. FUDMA Journal of Sciences 8(3):431–442. https://doi.org/10.33003/fjs-2024-0803-2486

Virbickaitė, A., Ausín, M. C., & Galeano, P. (2015). Bayesian inference methods for univariate and multivariate garch models: A survey. *Journal of Economic Surveys, 29*(1), 76–96. https://doi.org/10.1111/joes.12046

Virbickaitė, A., Ausín, M. C., & Galeano, P. (2016). A bayesian non-parametric approach to asymmetric dynamic conditional correlation model with application to portfolio selection. *Computational Statistics & Data Analysis, 100*, 814–829. https://doi.org/10.1016/j.csda.2014.12.005

Xiao, Y. H., Li, P. L., & Lu, S. (2021). Sparse estimation of high-dimensional inverse covariance matrices with explicit eigenvalue constraints. *Journal of the Operations Research Society of China, 9*, 543–568. https://doi.org/10.1007/s40305-021-00351-y

Zhou, S. L., Xiu, N. H., Luo, Z. Y., et al. (2015). Sparse and low-rank covariance matrix estimation. *Journal of the Operations Research Society of China, 3*(2), 231–250. https://doi.org/10.1007/s40305-014-0058-7

Authors and Affiliations

Zhangshuang Sun[1] · Qian Li[1] · Haixiang Lin[2] · Guoqiang Wang[1]

✉ Guoqiang Wang
guoq_wang@hotmail.com

Zhangshuang Sun
m440122108@sues.edu.cn

Qian Li
liqian15123329166@163.com

Haixiang Lin
H.X.Lin@tudelft.nl

[1] School of Mathematics, Physics and Statistics, Shanghai University of Engineering Science, Shanghai 201620, China

[2] Institute of Applied Mathematics, Delft University of Technology, Delft 2628 CD, the Netherlands